Universidade de São Paulo
Instituto de Física

Estados eletrônicos do ânion de resveratrol e suas subunidades

Ely Giancoli Ferreira de Miranda

Orientador: Prof. Dr. Márcio Teixeira do Nascimento Varella

Dissertação de mestrado apresentada ao Instituto de Física da Universidade de São Paulo, como requisito parcial para a obtenção do título de Mestre em Ciências.

Banca Examinadora:
Márcio Teixeira do Nascimento Varella (IF-USP)
Sergio d'Almeida Sanchez (IF-UFPR)
Mauricio Domingues Coutinho Neto (CCNH-UFABC)

São Paulo
2021

FICHA CATALOGRÁFICA
Preparada pelo Serviço de Biblioteca e Informação
do Instituto de Física da Universidade de São Paulo

Miranda, Ely Giancoli Ferreira de

Estados eletrônicos do ânion de resveratrol e suas subunidades. São Paulo, 2021.

Dissertação (Mestrado) – Universidade de São Paulo, Instituto de Física, Depto. de Física Geral

Orientador: Prof. Dr. Márcio Teixeira do Nascimento Varella

Área de Concentração: Física Atômica e Molecular

Unitermos: 1. Física Molecular; 2. Espalhamento; 3. Elétrons; 4. Antioxidantes; 5. Polifenóis

USP/IF/SBI-022/2021

University of São Paulo
Institute of Physics

Anionic states of resveratrol and its subunits

Ely Giancoli Ferreira de Miranda

Supervisor: Prof. Dr. Márcio Teixeira do Nascimento Varella

Dissertation submitted to the Physics Institute of the University of São Paulo in partial fulfillment of the requirements for the degree of Master of Science.

Examining Committee:
Márcio Teixeira do Nascimento Varella (IF-USP)
Sergio d'Almeida Sanchez (IF-UFPR)
Mauricio Domingues Coutinho Neto (CCNH-UFABC)

São Paulo
2021

Agradecimentos

Expresso aqui minha gratidão a todos e todas que possibilitaram a existência deste trabalho, produzido em um dos momentos mais difíceis da minha vida e de diversas pessoas, visto a pandemia de COVID-19. O presente trabalho foi realizado com apoio da Conselho Nacional de Desenvolvimento Científico e Tecnológico (CNPq), processo n° 131628/2019-4.

Visto isso, gostaria de agradecer ao CNPq pelo fomento ao meu projeto de mestrado desde o seu início, em 2019, a Comissão de Pós-Graduação do Instituto de Física (CPG) pela oportunidade de participação em um congresso. Também gostaria de agradecer ao Instituto de Física da Universidade de São Paulo (IFUSP), local onde descobri meu amor pela ciência e que construí amizades que levarei para toda minha vida. Aos amigos do IF, obrigado pelas discussões, pausas para o café, momentos de descontração e puxões de orelha.

Aos meus pais, Maria Lucia Giancoli e Eli Ferreira de Miranda agradeço pela confiança, apoio e motivação em toda essa caminhada. Muito obrigado por sempre me incentivarem a seguir o que eu amo. Vocês são os responsáveis por tudo isso e isso tudo é para vocês. Aos meus irmãos e irmãs, Deborah, Livia, Thiago, Daniel e Fábio, minhas tias Ana e Maria Cecília: um muito obrigado por sempre estarem dispostos e dispostas a uma boa conversa e, pelo apoio sempre presente. Tenho muita sorte de possuir uma família de sangue tão especial.

Agradeço também a minha família de coração, meus amigos de infância: Nicolas, Roberto, Gabriel, Pedro, Henrique e Giancarlo, que estão na caminhada comigo desde o início compartilhando ambições, experiências e momentos eternos.

Agradeço a Anna Beatriz Mendes Felix, por me aguentar nos momentos de loucura

e insegurança, por me motivar todos os dias a fazer o que eu amo e por me fazer sempre enxergar a vida a partir de um outro ponto de vista. Obrigado por tanto.

Por fim, agradeço ao grupo de pesquisa por sempre me receber de braços abertos e me ensinar tanto nesses últimos seis anos. Ao Lucas e ao Júlio por estarem comigo desde o começo, me ensinando todo o "abc" da área. E finalmente, ao Prof. Dr. Márcio Teixeira do Nascimento Varella, pelo apoio, conselhos, discussões, orientação e, principalmente, por toda inspiração que provoca.

Divido essa conquista com todos vocês, muito obrigado.

Ely Giancoli Ferreira de Miranda.

"Eu sou o sonho dos meus pais, que eram sonhos dos avós
Que eram sonhos dos meus ancestrais
Vitória é sonho dos olhares, que nos aguardam nos lares
Crendo que na volta somos mais"
(Emicida)

Resumo

Esse trabalho apresenta o primeiro estudo dos estados aniônicos de baixa energia do Resveratrol (RV) e Resorcinol (RS) através de técnicas de estado ligado e espalhamento. O RV representa um sistema muito desafiante computacionalmente devido ao seu tamanho. Nossos resultados apontaram um estado de valência ligado, três ressonâncias de forma e uma ressonância de caráter misto. Os limiares de dissociação (sem efeitos termodinâmicos) presentes na literatura e o espectro ressonante obtido são consistentes com resultados experimentais de espectroscopia de massa. Em particular, a produção de H_2 (produto da dissociação que pode ser responsável pela atividade antioxidante) para energias muito próximas de zero poderia ser proveniente de ressonâncias vibracionais de Feshbach decorrentes do estado ligado de valência. Também investigamos a subunidade RS do RV, que representa um protótipo computacionalmente mais viável para a produção de H_2. Obtivemos duas ressonâncias de forma e uma ressonância de caráter misto. Observamos que existe uma correspondência entre os estados aniônicos de RV e RS, até mesmo entre os limiares de dissociação, mas a falta de um estado ligado do ânion para as moléculas menores deve suprimir o canal de formação de H_2 em 0 eV.

Palavras-chave: antioxidantes, elétrons, espalhamento, ressonâncias, Resveratrol, Resorcinol, estados aniônicos, multicanal de Schwinger, sistemas polifenólicos.

Abstract

We report the first characterization of the anion states related to the dissociative processes in two compounds, Resveratrol (RV) and Resorcinol (RS), employing both scattering and bound states techniques. RV is a very challenging system for this kind of study in view of its size. Our results point out a valence bound state, three shape resonances and a mixed-character resonance. The zero-energy thresholds reported elsewhere and the presently calculated resonance spectrum are consistent with the mass spectroscopy data. In particular, with the production of H_2 (reaction that could account for the antioxidant activity) at nearly zero energy which could proceed from a vibrational Feshbach resonances arising from a valence bound state. We also investigated the RS subunit of the RV, which could be a less computationally expensive prototype for the production of H_2. We obtained two shape resonances and a mixed-character resonance. There is a correspondence between the anion states of RV and RS, and even between the thresholds, but the lack of anion bound states for the smaller molecules should suppress the H_2-formation channel at 0 eV.

Keywords: antioxidants, electrons, scattering, resonances, Resveratrol, Resorcinol, anionic states, low-energy, Schwinger multichannel, polyphenolic.

List of Figures

List of Tables

Contents

Chapter 1

Introduction

Several processes relevant to different science fields involve the interactions of electrons with atoms, molecules and materials [1–4]. The results of this interaction is different depending on the collision energy. At low energies (< 15 eV), for example, the electron-molecule collisions often involve the formation of transient negative ions, also called resonances. Resonances can be viewed as anion states whose energies are above of its ionization threshold. They correspond to an unbound discrete states embedded and coupled to the continuum of scattering states, which amount to nonzero auto-ionization probabilities for the quasi-discrete states. The formation of resonances is relevant to several fields, such as atmospheric sciences, the physics of processing plasmas and biochemistry [3, 5, 6].

In this work, we are interested in a particular application related to the antioxidants activity of polyphenolic compounds, motivated by recent experimental results [7] and potential medical and biological applications [8]. We studied the low-energy electron attachment in two polyphenolic compounds and show a pathway which can trigger its antioxidant effect. Bellow, we present an overview of the electronic capture problem and its subsequent processes.

1.1 Electron-Molecule Interaction

Electron-molecule scattering can be understood as a collisional process resulting from an interaction between a projectile (electron) and a target (molecule) at a finite region of space (associated by the interaction reach). The system final state emerges from an asymptotic limit and any possible configuration is called a *channel*. According to the final target state, there are many different channels such as elastic, inelastic or dissociative. A given target asymptotic configuration is only allowed if the incident electron energy is sufficient to form it. The allowed energy states define the *open channels*, other states being *closed* [9].

Experimentally, a collimated electron beam with well-defined initial kinetic energy is passed through a collision cell filled with the compound under investigation. The connection between a scattering measurement and theory is made through a quantity known as the scattering cross-section. The scattering cross-section is proportional to the rate at which a particular projectile-target interaction occurs, more specifically, it is a scattering rate (number of scattering events per unit time) per unit of incident projectile flux (number of incident particles striking the target surface per unit time per unit area) [9]. Measures can be made using electron transmission spectroscopy (ETS) experimental set [1].

The formation of a resonance appear as sharp fluctuations of the total electron-molecule scattering cross section as a function of the incident electron energy [10]. Fundamentally a resonant state has a finite life time which is characterized by a complex energy $E = E_R - i\Gamma/2$ where E_R is the resonance energy and Γ is the state auto-ionization width whose is associated with its life time $\gamma = \hbar/\Gamma$. In that way, the attach electron anion state is called a *transient negative ion* (TNI) because it is unstable against auto-ionization.

The TNIs can transfer the electronic energy into the vibrational degrees of freedom, thus triggering a dynamical process that can lead to the dissociation of the molecular anion. Since this procedure compete with auto-ionization, a bigger TNIs lifetime raises the dissociation probability. We call this process *dissociative elec-*

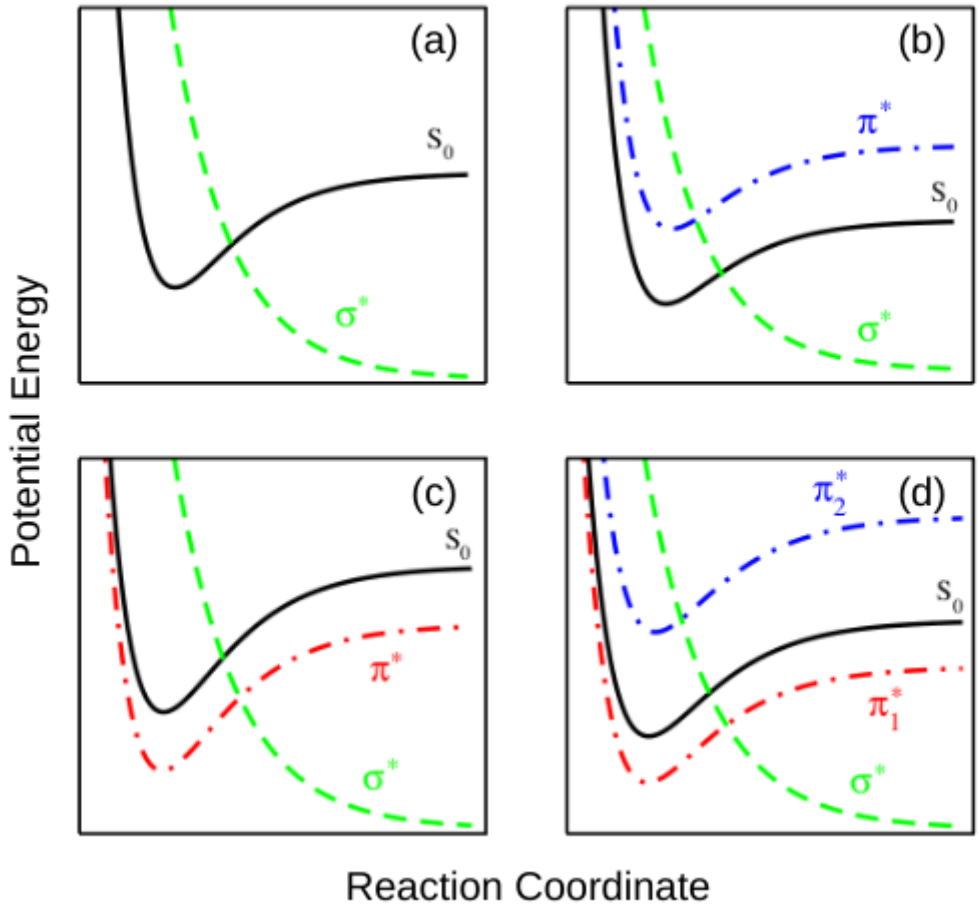

Figure 1.1: Potential energy surface scheme in function of a determinate reaction coordinate. (a) The black curve (S_0) denotes the ground state electronic energy of neutral molecule and the dotted curve represents a anti-bounded electronic anion state σ^*. (b) Two anion states represented by dashed green and blue curves. In that case, blue curve picture a π^* anion state. (c) Similar to (a) with a difference that the anion state is at lower energies than the neutral S_0 (red dashed curve). (d) Three different anion states, named π_1^*, π_2^* and the anti-bounded σ^*. Adapted from Ref. [11].

tron attachment (DEA). There are DEA formalities [12] but here we only provide a qualitative picture. If the dissociation is initiated by electron capture into an anti-bonding orbital with dissociative/repulsive character, we call this DEA process *direct*. Schematic potential energy surfaces relevant to this mechanism are presented as function of the generic reaction coordinate in Fig. 1.1a. The potential energy of the target ground state is indicated as S_0, and the system undergoes a transition to the anion state potential σ^* (green curve) by the electron attachment.

The *indirect* DEA mechanism is also represented in Fig. 1.1b. In this case, the electron capture gives rise to a non-dissociative resonance with π^* character (blue curve). The dissociation proceeds through the coupling between the π^* resonance and the σ^* one [12]. The c and d panels represent similar circumstances illustrating a possibility of a bounded anion state (red line) which can also lead a dissociative picture by the same process.

In next section we show how this process could appears in the biological systems and motivate the study of some compounds which the DEA process can trigger several effects.

1.2 Motivation and Biological Relevance

Life in our planet relies on two fundamental process: respiration and photosynthesis. They represent the means for the cellular energy production which is necessary for the living organisms [13]. Both process are inseparably linked with the presence of electrons moving through biological matter [14]. This balance is fulfilled along electron transfer pathways, in particular the mitochondrial *electron transport chains* (ETCs) [15]. Exogenous compounds may affect the delicate balance of those processes and could lead to disease conditions [10].

The mitochondrial ETC also produces *reactive oxygen species* (ROS), which have a adverse effect to cell health. Oxygen reduction generates the anionic super-oxide, $O_2 + e^- \rightarrow O_2^{-\bullet}$, which can result in an oxidative condition [16]. Pathologies such as cardiovascular diseases, Alzheimer's, Parkison's and cancer can be triggered by failures in the mitochondrial processes [17] attributed to ROS inter-membrane formation due to electron "leaking" from ETC [18]. ROS act as efficient oxidative substances capable of breaking the mithocondrial membranes, attacking DNA and causing mutations [19]. However, the ROS production can also leads to beneficial results in the cell, as producing oxidative damage in pathologies and performing cellular signaling [16]. Self-defense mechanisms that neutralize ROS are linked with generation of native antioxidants or include enzymatic protection. Therefore, it is believed that

oxireductive balance perturbations into mithocondrial inter-membrane can trigger significant cellular damage [10].

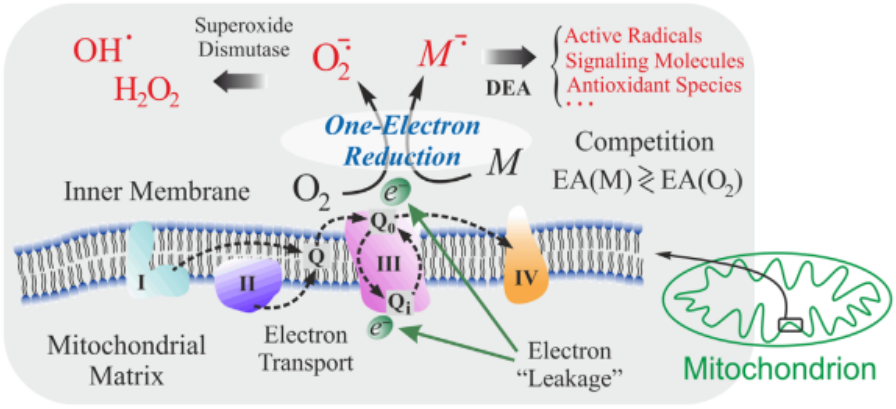

Figure 1.2: Analogy between the "leaked" electron attachment to cellular oxygen (O_2) and xenobiotic molecule (M) near Q_0 or Q_1 sites of the Complex III from the energy production cycle, located in the inner mitochondrial membrane. Membrane complexes of the ETC are labeled with roman numerals: I – NADH dehydrogenase, II – succinate, dehydrogenase, III – cytochrome bc1 complex, IV – cytochrome c oxidase. Q stands for ubiquinone, EA = electron affinity. Adapted from Ref. [10].

An efficient way to assist cell defense against ROS damage is the introduction of xenobiotic substances (non-native organism substances), with *electron affinities* (EAs) comparable to that of molecular oxygen - 0.45 eV in the gas phase -, where ROS concentration is abundant, as in the Complex III (Fig. 1.2). Since the ROS formation is initiated by the production of super-oxide anion-radical via one-electron reduction of cellular oxygen by electrons "leaked" from the mitochondrial electron transport chains [20, 21], any molecule with significant EA can compete with the O_2 molecule for electron capture (Fig. 1.2). Relatively small molecules (atomic wights below than 1500 atomic units) can easily penetrate the outer mitochondrial membrane [22]. These xenobiotic compounds could compete for electrons "leaked" from the respiratory chain and regulate the ROS generation. The electron transfer to alien species likely occurs in the presence of O_2 for energetic reasons, in other words the EA of a xenobiotic molecule has to be close (or exceeds) to that of molecular oxygen [23]. After the capture, we expact that the xenobiotic compund suffers a DEA process which triggers the production of secondary species that could be beneficial (antioxidant species and signaling molecules) or maleficial (active orbitals) to cell, as

shown in Fig. 1.2.

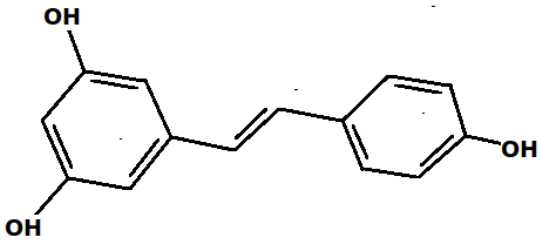

Figure 1.3: Structure of Trans-Resveratrol.

Fig. 1.3 reports the RV molecule, a naturally occurring plant phytoalexin and a constituent of red wine, well-known for its strong antioxidant activity. The RV produces beneficial effects in human health by preventing a variety of illnesses as: cancer, cardiovascular malfunction, neurodegenerative diseases, inflammation, and atherosclerosis [8]. However, the molecular mechanisms underlying the bioactivity of RV resulting in this variety of beneficial effects is not well understood [8]. In general, the useful effects of natural polyphenolic compounds are associated with their antioxidant properties related to two main mechanisms for the scavenging of free radicals: H-atom abstraction and electron removal [24]. The first is attributed from a H abstraction at hydroxyl groups site and its transference to reactive species, in order to interrupt the chain reaction of lipid peroxidation, governed by the rate of OH bond cleavage. The second mechanism is associated with the electron removal from antioxidant molecules, forming radical cations followed by rapid deprotonation, which is governed by the ionization potential.

Polyphenolic antioxidants, such as flavonoids and spinochromes, are good electron acceptors [25] and can interact with electrons under reductive conditions in cells. The DEA reaction with multiple substituted OH aromatic compounds has been found to efficiently produce doubly dehydrogenated anions and H_2 neutral species [25]. It has been reported that the H_2 gas is one of the simplest antioxidant species and has been successfully used clinically [26].

Recently, a new molecular mechanism for the antioxidant activity of the polyphenolic compound RV is proposed [7]. This mechanism explore the xenobiotic reduction

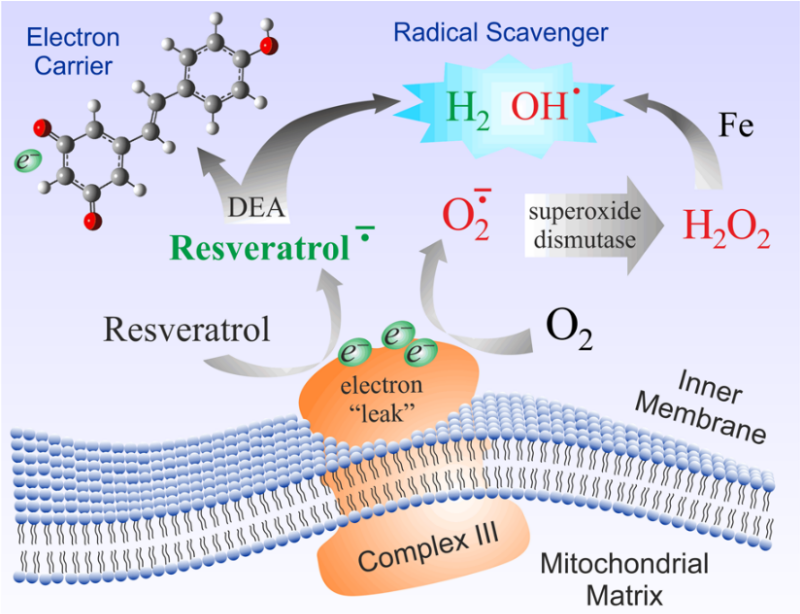

Figure 1.4: Schematic representation of the likely resveratrol activity in the intermembrane space: formation of a temporary negative ion by the attachment of "leaked" electrons, followed by the generation of the semiquinone and the neutral H_2 radical scavenger via the DEA mechanism in vivo. Adapted from Ref. [7].

possibility in the mitochondrial intermembrane space by electron "leaking" (Fig. 1.4). This possibility has been recently demonstrated with the anthralin and antipsoriatic drug activity in the mitochondria of keratinocytes [27]. The hypothesis suggests that the generation of neutral H_2 molecules is likely to involve DEA with polyphenolic compounds.

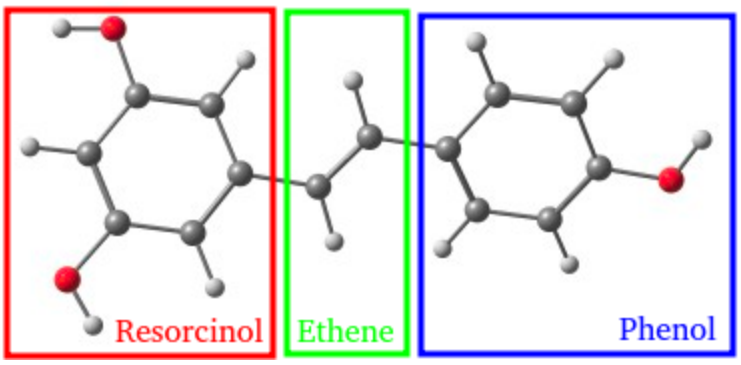

Figure 1.5: Schematic representation of the molecular subunits.

Since the H and H_2 generation can be trigged by a DEA process, scattering techniques were utilized to characterize the RV anionic states. One of the main difficulties in the theoretical description of RV anionic states is the computational

effort arising from the size and lack of symmetry elements. The RV molecule has 29 atoms, which is considered large for this type of calculations. The H elimination from hydroxyl groups would be expected in view of the strong polar character of the bonds, thus H-atom abstraction shall preferably occur in the PH and RS polyphenolic subunits (Fig. 1.5). PH anionic states are already studied in literature [2], in contrast to RS which should be the responsible for the H_2 formation of RV, since it has two hydroxyl groups.

RS is been widely known as a versatile chemical compound utilized extensively in the development of advanced chemical industry [28]. The molecule has two hydroxyl groups in the aromatic ring structure, and they are located at their meta-positions with respect to each hydroxyl group. The excited state dynamics of neutral polyphenolic compounds has been largely studied theoretically and experimentally [29], with considerable attention to the elimination of H atoms from hydroxyl groups. In contrast, we are not aware of similar theoretical studies for the anion states. In that way, RS is an interesting system to study with a more accessible computational effort.

Therefore, we employ scattering techniques to investigate the RV and RS anion states, in order to analyze the H_2 production through a DEA process. The subunit investigation can present a good way to avoid a high computational effort, allowing an establishment of a methodology for the study of complex molecules. The present investigation may shed some light on the mechanism of biochemical reactions under reductive conditions and the therapeutic effects of polyphenolic compounds.

1.3 The Dissertation

This dissertation is organized as follows: In Chapter II we present the bound state theoretical methods employed for the characterization of the neutral molecules. In Chapter III scattering theory will be presented through the *Schwinger Multichannel Method* (SMC), which was used to solve the electron-molecule scattering problem. Chapter IV reports the bound state results for RS and RV molecules. Finally, the scattering and dissociation thresholds results are presented in Chapter 5.

Chapter 2

Theoretical Methods I: Molecular Bound States

In this chapter I will briefly present the theoretical methods employed to characterize the bound states of atoms and molecules quantum mechanically. It is important to highlight the difficult to deal with many-body interacting systems, as they are typically composed of a large number of electrons. The methods used in this work will be outlined in the following sections and the details can be found elsewhere [30–32].

Since the interaction between nuclei and electrons can be described by the Coulomb Law, the starting point is time-independent Schrödinger equation for a molecule with M nuclei and N electrons

$$\mathscr{H}\left|\Psi\right\rangle = E\left|\Psi\right\rangle, \tag{2.1}$$

in which $|\Psi\rangle$ represents the systems state. The wave function is obtained by projection onto the *bra* vector, $\Psi\left(\mathbf{R},\mathbf{r}\right) = \langle\mathbf{R},\mathbf{r}|\Psi\rangle$, where $\mathbf{R}$ represents the $3M$ nuclear-space coordinates and $\mathbf{r}$ the $3N$ electronic-space coordinates. The Hamiltonian $\mathscr{H}$ is characterized by

$$\mathscr{H} = T_N + T_e + V_{Ne} + V_e + V_N, \tag{2.2}$$

where T_N and T_e represent nuclear and electronic kinetic energy operators, while V_{Ne}, V_e and V_N denote the electron-nucleus, electron-electron and nucleus-nucleus Coulomb potential energy operators, respectively. We can write these operators in

atomic units ($m_e = \hbar = e = (4\pi\epsilon_0)^{-1} = 1$) as follows

$$\mathscr{H} = -\sum_{\mu=1}^{M} \frac{1}{2M_\mu}\nabla_\mu^2 - \frac{1}{2}\sum_{i=1}^{N}\nabla_i^2 - \sum_{i,\mu}\frac{Z_\mu}{R_{i\mu}} + \sum_{i,j}\frac{1}{r_{ij}} + \sum_{\mu,\nu}\frac{Z_\mu Z_\nu}{R_{\mu\nu}}, \tag{2.3}$$

where $M_\mu(Z_\mu)$ is the μ-th nucleus mass (charge); $R_{i\mu}$, r_{ij} and $R_{\mu\nu}$ indicate electron-nucleus, electron-electron and nucleus-nucleus distances defined by $|\mathbf{r}_i - \mathbf{R}_\mu| \equiv R_{i\mu}$, $|\mathbf{r}_i - \mathbf{r}_j| \equiv r_{ij}$ e $|\mathbf{R}_\mu - \mathbf{R}_\nu| \equiv R_{\mu\nu}$ where we use $\mathbf{r}_i$ and $\mathbf{R}_\mu$ to denote i-th electron and μ-th nucleus position, respectively; and the ∇_i^2 and ∇_μ^2 operators correspond to the $\mathbf{r}_i$ and $\mathbf{R}_\mu$ laplacians.

We have the complex task to solve Eq. 2.1 which, in fact, does not have an analytical solution. We will need to use approximations, starting from the Born-Oppenheimer (BO) separation to decouple the electronic and nuclear dynamics.

2.1 Born-Oppenheimer Approximation

The BO separation is usually considerate as the starting point to treat molecular systems. The essential idea is to decouple the electronic and nuclear motions. The motivation is based on the fact that nuclear masses are way larger than the electron mass, which originates a dynamical notable motion disparity. Spectroscopic measurements justify this tendency showing that electrons approximately move in the field of fixed nuclei [33]. Mathematically the BO separation for the system is written as

$$|\Psi\rangle = |\Phi\rangle \otimes |\psi\rangle \Longrightarrow \Psi(\mathbf{R}, \mathbf{r}) = \Phi(\mathbf{R})\,\psi(\mathbf{r}|\mathbf{R}), \tag{2.4}$$

where $|\Phi\rangle$ ($\Phi(\mathbf{R})$) and $|\psi\rangle$ ($\psi(\mathbf{r}|\mathbf{R})$) represent the nuclear and electronic state (wave function) respectively. The electronic wave function explicitly depend on the electronic coordinates for a given fixed configuration of the nuclei, i.e., there is a parametric dependence on $\mathbf{R}$.

The next step is to use BO separation form from Eq. 2.4 into Eq. 2.1. But first let us take a look again into Eq. 2.2: We decompose the system Hamiltonian into

two groups. The first one is $\mathscr{H}_e \equiv T_e + V_{Ne} + V_e$, which only includes the electronic operators, , and the second one is $\mathscr{H}_N \equiv T_N + V_N$ which is composed by only nuclear operators. In that way we separate Eq. 2.2 as follows

$$\Phi(\mathbf{R})\left[\mathscr{H}_e\ \psi(\mathbf{r}|\mathbf{R})\right] + \psi(\mathbf{r}|\mathbf{R})\left[\mathscr{H}_N\ \Phi(\mathbf{R})\right] = E\ \Phi(\mathbf{R})\,\psi(\mathbf{r}|\mathbf{R}), \tag{2.5}$$

in which the electronic part is

$$\mathscr{H}_e\ \psi(\mathbf{r}|\mathbf{R}) = \epsilon(\mathbf{R})\ \ \psi(\mathbf{r}|\mathbf{R}), \tag{2.6}$$

which can, in principle, be solved and thus generates a family of orthonormal functions $\psi_m(\mathbf{r}|\mathbf{R})$ with $m = 0, 1, 2, ...$ associated to the eigenvalues $\epsilon_m(\mathbf{R})$ since $\mathscr{H}_e$ is hermitian. In that regime, the energy associated with a given certain electronic state m is described as a M-dimensional hypersurface

$$E_m(\mathbf{R}) = \epsilon_m(\mathbf{R}) + \sum_{\upsilon=1}^{M}\sum_{\mu<\upsilon}^{M}\frac{Z_\upsilon Z_\mu}{|\mathbf{R}_\upsilon - \mathbf{R}_\mu|}. \tag{2.7}$$

Therefore we could use this orthonormal family of solutions to rewrite $\psi(\mathbf{r}|\mathbf{R}) = \sum_m \alpha_m(\mathbf{R})\,\psi_m(\mathbf{r}|\mathbf{R})$, where $\alpha_m(\mathbf{R}) = \langle\psi_m|\psi\rangle$, which inspire a new way to write BO separation:

$$\Psi(\mathbf{R},\mathbf{r}) = \sum_m \Phi_m(\mathbf{R})\,\psi_m(\mathbf{r}|\mathbf{R}), \tag{2.8}$$

know as the Born-Huang Expansion [34] and the coefficients $\Phi_m(\mathbf{R})$ are interpreted as a enumerable family of nuclear wave functions. In order to determinate those coefficients and consequently describe the nuclear motion we substitute Eq. 2.8 into Eq. 2.5 obtaining

$$\sum_m\left[-\sum_{\mu=1}^{M}\frac{1}{2M_\mu}\nabla_\mu^2 + (\epsilon_m(\mathbf{R}) - E)\right]\Phi_m(\mathbf{R})\,\psi_m(\mathbf{r}|\mathbf{R}) = 0. \tag{2.9}$$

Then, we project above equation into an electronic state $\psi_m(\mathbf{r}|\mathbf{R})$. Before doing so,

it is convenient to introduce the notation

$$(\nabla_\mu)_{nm} \equiv \langle\psi_n|\nabla_\mu|\psi_m\rangle = \int d\mathbf{r}\ \psi_n^*(\mathbf{r}|\mathbf{R})\,\nabla_\mu\psi_m(\mathbf{r}|\mathbf{R}), \tag{2.10}$$

which also applies for ∇_μ^2. In that way we obtain

$$\left(-\sum_{\mu=1}^{M}\frac{1}{2M_\mu}\nabla_\mu^2 - \sum_{\mu=1}^{M}\frac{1}{M_\mu}\left(\nabla_\mu^2\right)_{mm} + (\epsilon_m(\mathbf{R}) - E)\right)\Phi_m(\mathbf{R}) = \sum_{m\neq n}\sum_{\mu=1}^{M}\frac{1}{M_\mu}\left((\nabla_\mu)_{nm}\cdot\nabla_\mu + \frac{\left(\nabla_\mu^2\right)_{nm}}{2}\right)\Phi_m(\mathbf{R}). \tag{2.11}$$

The $(\nabla_\mu)_{nm}$ and $\left(\nabla_\mu^2\right)_{nm}$ diagonal matrix elements ($m = n$) are called adiabatic coupling terms while non-diagonal elements ($n \neq m$) are called non-adiabatic coupling terms. The adiabatic approximation considers negligible all non-adiabatic terms (non-diagonal terms) resulting in

$$\left(-\sum_{\mu=1}^{M}\frac{1}{2M_\mu}\nabla_\mu^2 + \epsilon_m(\mathbf{R}) - E + \sum_{\mu=1}^{M}\frac{1}{M_\mu}\left(\nabla_\mu^2\right)_{mm}\right)\Phi_m^{(ADA)}(\mathbf{R}) = 0, \tag{2.12}$$

where ADA stands for adiabatic approximation. This approximation define a vibrational nuclear motion, which arises from the electronic solution. We could also note that nuclear mass is much bigger than electronic mass, so the last term on the left-hand side of ADA is also negligible $\nabla_\mu^2/M_\mu \sim 0$ defining the BO approximation (BOA)

$$\left(-\sum_{\mu=1}^{M}\frac{1}{2M_\mu}\nabla_\mu^2 + \epsilon_m(\mathbf{R}) - E\right)\phi_m^{(BOA)}(\mathbf{R}) = 0. \tag{2.13}$$

It is possible to demonstrate that matrix elements in Eq. 2.10 satisfy, for $n \neq m$, the following relation

$$\left(\nabla_\mu^2\right)_{nm} = (\nabla_\mu)_{nm}^2 + \nabla_\mu\cdot(\nabla_\mu)_{nm}. \tag{2.14}$$

It follows that non-adiabatic couplings depend essentially on the $(\nabla_\mu)_{nm}$ matrix element which is neglected in the ADA. On the other hand, this term is related to the

difference between electronic state energies and, can be rewritten as [35]

$$(\nabla_\mu)_{nm} = \frac{\langle \psi_n | \nabla_\mu \mathscr{H}_e | \psi_m \rangle}{U_n(\mathbf{R}) - U_m(\mathbf{R})}, \tag{2.15}$$

in which

$$U_n(\mathbf{R}) \equiv \epsilon_n(\mathbf{R}) - \sum_{\mu=1}^{M} \frac{1}{M_\mu} \left(\nabla_\mu^2\right)_{nn}. \tag{2.16}$$

The above result means that BOA and ADA approximations are valid in energetically distant electronic states regions. It is typically applicable to the ground state around the nuclear equilibrium geometry. However, for excited states or far from nuclear equilibrium geometry this approaches can be non-satisfactory. In general terms, the BOA provides a possibility to treat the electronic states with fixed nuclei. In the following, we discuss approximations to the electronic eigenstates.

2.2 Multi-Electronic Systems

The BO separation provides us a pure electronic problem with N indistinguishable electrons submitted to the fixed-nuclei field. As started above this problem generally does not have an analytical solution because it consists in an interactive many-body system, therefore we need to use approximations to solve it.

It is important to say that an electron is quantum mechanically defined by its orbital and its spin. The orbital part is described solving Eq. 2.6 and the spins part is constructed by imposing the antisymmetry relation, since it is a fermion. In order to build a many-electron state we use the Independent Particle Approximation which states that a system of electrons is construct on one-electron states. A one-electron state is build by a product between the orbital and spin vectors[1], defining a *spin-orbital*:

$$|\psi\rangle = |\mathscr{O}\rangle \otimes |\mathscr{S}\rangle \Longrightarrow \psi(\mathbf{r}_i) = \mathscr{O}(\mathbf{r}_i)\,\mathscr{S}(i), \tag{2.17}$$

where $|\mathscr{O}\rangle$ $(\mathscr{O}(\mathbf{r}_i))$ and $|\mathscr{S}\rangle$ $(\mathscr{S}(i))$ represent orbital and spin states (wave function)

[1] Rigorously this product is valid to atoms whose spin-orbit coupling is negligible.

respectively, and the index i refers to i-th electron. For a spin s particle its multiplicity is $2s+1$. So as electrons are fermions $s = 1/2$, there are only two possible configurations:

$$\mathscr{S}(i) = \begin{cases} \uparrow(i), & \text{which represents up spin,} \\ \downarrow(i), & \text{which represents down spin,} \end{cases} \tag{2.18}$$

where $\uparrow(i)$ and $\downarrow(i)$ are orthonormal. We need to construct a electronic wave function that respects Pauli Exclusion Principle, in other words that is antisymmetric when submitted the exchange of two electrons. An state that respects this antisymmetric propriety is the Slater Determinant written as a determinant composed of spin-orbitals:

$$\psi(\mathbf{r}) = \frac{1}{\sqrt{N!}} \begin{vmatrix} \psi_1(\mathbf{r}_1) & \psi_2(\mathbf{r}_1) & \dots & \psi_N(\mathbf{r}_1) \\ \psi_1(\mathbf{r}_2) & \psi_2(\mathbf{r}_2) & \dots & \psi_N(\mathbf{r}_2) \\ \vdots & \vdots & \ddots & \vdots \\ \psi_1(\mathbf{r}_N) & \psi_2(\mathbf{r}_N) & \dots & \psi_N(\mathbf{r}_N) \end{vmatrix}, \tag{2.19}$$

which denotes electrons populating N spin-orbitals and generating a multi-electronic wave function ψ where $\mathbf{r} = (\mathbf{r}_1, ..., \mathbf{r}_N)$ and

$$\psi_j(\mathbf{r}_i) = \mathscr{O}_j(\mathbf{r}_i)\,\mathscr{S}(i). \tag{2.20}$$

Defining a more compact form:

$$\psi_j(\mathbf{r}_i) \equiv \psi_j^{(i)},\ \mathscr{O}_j(\mathbf{r}_i) \equiv \mathscr{O}_j^{(i)}. \tag{2.21}$$

Note that Pauli Exclusion Principle is immediately satisfied in this determinant since the sign is inverted when lines or columns are interchanged. In general each molecular orbital can be occupied by only two electrons with different spin states. In that way if we have K orbitals we obtain $2K$ distinct spin-orbitals. So the total

number of available Slater determinants is determined by the binomial:

$$\binom{2K}{N} = \frac{(2K!)}{N!\,(2K-N)!}. \tag{2.22}$$

We need to determinate which molecular orbitals make Eq. 2.19 a solution for the electronic problem in Eq 2.6. There are many different electronic structure methods to calculate it, some of them are going to be shortly explained in the next sections.

2.3 Hartree-Fock-Roothan Method

The Hartree-Fock (HF) method is one of the oldest and more successful ways to calculate the electronic structure of atoms and molecules. It seeks an approximate solution for the ground state of the electronic system using a single Slater determinant. This solution is obtained from the variational theorem using a variational criteria:

$$E\left[\psi\right] = \frac{\langle\psi|\mathscr{H}_e|\psi\rangle}{\langle\psi|\psi\rangle}, \tag{2.23}$$

in other words we need to minimize energy functional in order to obtain our best N-electron wave function function $\psi\left(\mathbf{r}\right)$. By substituting the electronic Hamiltonian in Eq. 2.2 into Eq. 2.23 we obtain

$$E\left[\psi\right] = \sum_{i}^{N} h_i + \frac{1}{2}\sum_{i=1}^{N}\sum_{j=1}^{N}\left(J_{ij} - K_{ij}\right), \tag{2.24}$$

where

$$h_i \equiv \left\langle \psi_i^{(i)} \middle| h_i \middle| \psi_i^i \right\rangle = \left\langle \psi_i^{(i)} \middle| -\frac{1}{2}\nabla_i^2 - \sum_{\mu=1}^{M}\frac{Z_\mu}{R_{i\mu}} \middle| \psi_i^i \right\rangle, \tag{2.25a}$$

$$J_{ij} \equiv \left\langle \psi_i^{(i)}\psi_j^{(j)} \middle| \frac{1}{r_{ij}} \middle| \psi_i^{(i)}\psi_j^{(j)} \right\rangle, \tag{2.25b}$$

$$K_{ij} \equiv \left\langle \psi_i^{(i)}\psi_j^{(j)} \middle| \frac{1}{r_{ij}} \middle| \psi_j^{(i)}\psi_i^{(j)} \right\rangle \tag{2.25c}$$

whose h_i, J_{ij} and K_{ij} are the non-interacting, Coulomb and Exchange matrix elements, respectively. Note that the two last equations represent two particle integrals.

Next, we use a variational procedure to search for a extremum of the functional in Eq. 2.24 with respect to molecular spin-orbitals. We employ Lagrange Multipliers Method with orthonormal spin-orbitals constraint which generates a total of N^2 Lagrange Multipliers and the extremum condition become

$$\delta\left(E\left[\psi\right]-\sum_{i=1}^{N}\sum_{j=1}^{N}\epsilon_{ij}\left(S_{jk}-\delta jk\right)\right)=0, \tag{2.26}$$

in which

$$S_{ij}\equiv\left\langle\psi_i^{(i)}\middle|\psi_j^{(j)}\right\rangle \tag{2.27}$$

is the *Overlap integral*. After developing mathematically Eq. 2.26 we obtain a set of equations known as the HF equations:

$$F\left(i\right)\left|\psi_j^{(i)}\right\rangle=\sum_{k=1}^{N}\epsilon_{kj}\left|\psi_j^{(i)}\right\rangle, \tag{2.28}$$

where $F\left(i\right)$ is the *Fock Operator* that corresponds to the mean-field produced by other $(N-1)$ electrons and is defined by other operators

$$F\left(i\right)\equiv h\left(i\right)+\frac{1}{2}\sum_{k=1}^{N}\left(\mathscr{J}_i\left(i\right)-\mathscr{K}_i\left(i\right)\right), \tag{2.29}$$

where $\mathscr{J}_k\left(i\right)$ and $\mathscr{K}_k\left(i\right)$ are the Coulomb and Exchange operators respectively and, their operations on the spin-orbitals are given by

$$\mathscr{J}_k\left(i\right)\left|\psi_i^{(j)}\right\rangle=\left\langle\psi_n^{(k)}\right|\frac{1}{r_{in}}\left|\psi_n^{(k)}\right\rangle\left|\psi_i^{(j)}\right\rangle, \tag{2.30a}$$

$$\mathscr{K}_k\left(i\right)\left|\psi_i^{(j)}\right\rangle=\left\langle\psi_n^{(k)}\right|\frac{1}{r_{in}}\left|\psi_n^{(j)}\right\rangle\left|\psi_i^{(k)}\right\rangle. \tag{2.30b}$$

The Lagrange Multipliers ϵ_{ij} are matrix elements of a hermitian operator $\bar{\epsilon}$, therefore there is an unitary transformation U such that $\bar{\epsilon}^*=U^\dagger\bar{\epsilon}U$ is diagonal with real

elements. So we conclude that the molecular orbitals satisfy

$$F(i)\left|\psi_i^{(j)}\right\rangle = \epsilon_j \left|\psi_i^{(j)}\right\rangle, \tag{2.31}$$

with $\epsilon_j \equiv \epsilon_{jj}$.

The Eqs. 2.31 for $j = 1, 2, ...$ are know as the Canonical HF Equations and defines the molecular spin-orbitals that minimize the electronic energy functional with the eigenvalues ϵ's associated to the orbital energies. As the Fock equations are a set of coupled integro-differential equations, they are solved by an interactive process called *Self-Consistent Field* (SCF). In this procedure the spin-orbitals are generated iteratively, i.e., given some spin-orbitals initial guess, Eq. 2.31 is solved generating a new set of spin-orbitals, then this new set is choosen as an initial guess and Eq. 2.31 is solved again, generating another spin-orbitals set, and so on. This procedure is repeated until a predefined conversion is matched.

For closed shell molecules each orbital is occupied by two electrons with opposite spins, which allows the HF Canonical Equations to be expressed only in terms of the molecular orbitals. This simplified method is called *Restricted Hartree-Fock* (RHF),

$$F(i)\left|\mathscr{O}_i^{(j)}\right\rangle = \epsilon_j \left|\mathscr{O}_i^{(j)}\right\rangle, \;\; j = 1, 2, ..., N/2. \tag{2.32}$$

In this case the Fock Operator is

$$F(i) \equiv h(i) + \sum_{k=1}^{N/2} \left(2\mathscr{J}_k(i) - \mathscr{K}_k(i)\right), \tag{2.33}$$

with Coulomb and Exchange operators given by:

$$\mathscr{J}_k(i)\left|\mathscr{O}_i^{(j)}\right\rangle = \left\langle \mathscr{O}_i^{(k)}\left|\frac{1}{r_{in}}\right|\mathscr{O}_i^{(k)}\right\rangle \left|\mathscr{O}_i^{(j)}\right\rangle, \tag{2.34a}$$

$$\mathscr{K}_k(i)\left|\mathscr{O}_i^{(j)}\right\rangle = \left\langle \mathscr{O}_i^{(k)}\left|\frac{1}{r_{in}}\right|\mathscr{O}_i^{(j)}\right\rangle \left|\mathscr{O}_i^{(k)}\right\rangle. \tag{2.34b}$$

These expressions are similar to the more general ones in Eqs. 2.31 although restricted

to the orbital space. Therefore the SCF cycles in the RHF method only seeks for molecular orbitals.

For open shell molecular systems the electrons number N is odd. The method of solving the electronic problem is usually the *Unrestricted Hartree-Fock* (UHF). The UHF method proposed by Pople-Nesbet splits the electrons into two clusters: $n_\uparrow$ for up spin electrons and $n_\downarrow$ for down spin electrons, such that $n_\uparrow + n_\downarrow = N$. The energy expectation value can be expressed as

$$E\left[\psi\right] = \sum_{q=1}^{n_\uparrow} \left\langle \psi_q^\uparrow \middle| h \middle| \psi_q^\uparrow \right\rangle + \frac{1}{2} \sum_{q,l=1}^{n_\uparrow} \left\langle \psi_q^\uparrow \middle| \mathscr{J}_{l\uparrow} - \mathscr{K}_{l\uparrow} \middle| \psi_q^\uparrow \right\rangle + \sum_{q=1}^{n_\downarrow} \left\langle \psi_q^\downarrow \middle| h \middle| \psi_q^\downarrow \right\rangle +$$

$$+ \frac{1}{2} \sum_{q,l=1}^{n_\downarrow} \left\langle \psi_q^\downarrow \middle| \mathscr{J}_{l\downarrow} - \mathscr{K}_{l\downarrow} \middle| \psi_q^\downarrow \right\rangle + \frac{1}{2} \sum_{q,l=1}^{n_\uparrow, n_\downarrow} \left\langle \psi_q^\uparrow \middle| \mathscr{J}_{l\downarrow} \middle| \psi_q^\uparrow \right\rangle + \frac{1}{2} \sum_{q,l=1}^{n_\downarrow, n_\uparrow} \left\langle \psi_q^\downarrow \middle| \mathscr{J}_{l\uparrow} \middle| \psi_q^\downarrow \right\rangle \quad (2.35)$$

where the $\left|\psi_q^\uparrow\right\rangle$ and $\left|\psi_q^\downarrow\right\rangle$ states are associated to the $\left|\mathscr{O}_q\right\rangle\left|\uparrow\right\rangle$ and $\left|\mathscr{O}_q\right\rangle\left|\downarrow\right\rangle$ spin-orbitals respectively. The $\mathscr{J}_{q^\xi}$ and $\mathscr{K}_{q^\xi}$ operators, for $\xi = \uparrow$ and $\downarrow$, are defined as follow

$$\mathscr{J}_{q^\xi}\left(i\right) \left| \psi_i^{(l^\xi)} \right\rangle = \left\langle \psi_n^{(q^\xi)} \middle| \frac{1}{r_{in}} \middle| \psi_n^{(q^\xi)} \right\rangle \left| \psi_i^{(l^\xi)} \right\rangle, \quad (2.36a)$$

$$\mathscr{K}_k\left(i\right) \left| \psi_i^{(l^\xi)} \right\rangle = \left\langle \psi_n^{(q^\xi)} \middle| \frac{1}{r_{in}} \middle| \psi_n^{(l^{\xi^*})} \right\rangle \left| \psi_i^{(q^\xi)} \right\rangle. \quad (2.36b)$$

The procedure for functional minimization is similar, but the orthogonality condition is recast as

$$S_{ql}^{\xi\xi^*} \equiv \left\langle \psi_{q^\xi} \middle| \psi_{l^{\xi^*}} \right\rangle = \delta_{ql}\delta_{\xi\xi^*}, \quad (2.37)$$

such that

$$\delta\left(E\left[\psi\right] - \sum_{q=1}^{n_\uparrow} \epsilon_q^\uparrow \left(S_{qq}^{\uparrow\uparrow} - 1\right) - \sum_{q=1}^{n_\downarrow} \epsilon_q^\downarrow \left(S_{qq}^{\downarrow\downarrow} - 1\right) \right) = 0 \quad (2.38)$$

resulting into the equations:

$$\mathscr{F}_\uparrow\left(i\right) \left| \psi_i^{(q^\uparrow)} \right\rangle = \epsilon_q^\uparrow \left| \psi_i^{(q^\uparrow)} \right\rangle, \quad (2.39a)$$

$$\mathscr{F}_\downarrow\left(i\right) \left| \psi_i^{(q^\downarrow)} \right\rangle = \epsilon_q^\downarrow \left| \psi_i^{(q^\downarrow)} \right\rangle. \quad (2.39b)$$

in which

$$\mathscr{F}_{\uparrow}(i) = h(1) + \sum_{l=1}^{n_{\uparrow}} \left(\mathscr{J}_{l\uparrow}(i) - \mathscr{K}_{l\uparrow}(i) \right) + \sum_{l=1}^{n_{\downarrow}} \mathscr{J}_{l\downarrow}(i), \tag{2.40a}$$

$$\mathscr{F}_{\downarrow}(i) = h(1) + \sum_{l=1}^{n_{\downarrow}} \left(\mathscr{J}_{l\downarrow}(i) - \mathscr{K}_{l\downarrow}(i) \right) + \sum_{l=1}^{n_{\uparrow}} \mathscr{J}_{l\uparrow}(i). \tag{2.40b}$$

The SCF cycles are performed for the two spin-orbitals initial sets - one for each spin. As the solutions are different for the spin components, the UHF method is also called polarized spin method. It is also important to note that $|\psi\rangle$ is not necessarily a S^2 eigenstate.

The HF orbitals are usually expanded as *Linear Combination of Atomic Orbitals* (LCAO). In practice we choose a prior set of n normalized atomic orbitals $\{\lambda_\mu\}$ and use them as a basis to expand the molecular orbitals

$$|\mathscr{O}_i\rangle = \sum_{\mu=1}^{n} C_{i\mu} |\lambda_\mu\rangle \tag{2.41}$$

in which $\langle\lambda_\mu|\lambda_\mu\rangle = 1$. It is convenient to write Eq. 2.41 in vectorial and matrix notation as

$$\begin{pmatrix} |\mathscr{O}_1\rangle \\ |\mathscr{O}_2\rangle \\ \dots \\ |\mathscr{O}_N\rangle \end{pmatrix} = \begin{pmatrix} C_{11} & C_{12} & \dots & C_{1n} \\ C_{21} & C_{22} & \dots & C_{2n} \\ \dots & \dots & \dots & \dots \\ C_{N1} & C_{N2} & \dots & C_{Nn} \end{pmatrix} \begin{pmatrix} |\lambda_1\rangle \\ |\lambda_2\rangle \\ \dots \\ |\lambda_n\rangle \end{pmatrix} \tag{2.42}$$

with $\mathbf{C} = (C_{i\mu})$. Using Eq. 2.41 in Eq. 2.31 and applying $\langle\lambda_\nu|$ on the left side, we obtain equations for the $C_{i\mu}$ coefficients:

$$\mathbf{FC} = \mathbf{SC}\epsilon, \tag{2.43}$$

where $\epsilon = (\epsilon_{ij}) = (\epsilon_i \delta_{ij})$, $\mathbf{F} = (F_{\mu\nu})$ and $\mathbf{S} = (S_{\mu\nu})$, with

$$F_{\mu\nu} = \langle \lambda_\mu | F | \lambda_\nu \rangle \,, \tag{2.44a}$$

$$S_{\mu\nu} = \langle \lambda_\mu | \lambda_\nu \rangle \,. \tag{2.44b}$$

The Eq. 2.43 can be written as:

$$(\mathbf{F} - \epsilon \mathbf{S})\, \mathbf{C} = 0 \tag{2.45}$$

which represents a set of equations know as Hatree-Fock-Roothan (HFR) equations:

$$\sum_{\mu=1}^{n} (F_{\mu\nu} - \epsilon_i S_{\mu\nu})\, C_{\mu i} = 0 \tag{2.46}$$

for $i = 1, 2, ..., N$ and $\nu = 1, 2, ..., n$. The HFR eigenvalues are roots of the secular equation

$$\det |\mathbf{F} - \epsilon \mathbf{S}| = 0 \tag{2.47}$$

which is self-consistent solved with a SCF cycle.

The main limitation of the in HF method is the inability to treat the dynamical electronic correlation energy which is related to the electronic repulsion energy associated with moving electrons. In the HF solution, each electron only experiences the mean-filed potential due to the other ones. To overcome this problem we need to resort to more sophisticated techniques, called post-HF methods, which incorporate the dynamical electronic correlation energy based on the HF solution. One of them is the Møller-Plesset second order perturbation theory (MP2) which the electronic correlation is included via second order perturbation theory [30]. In the next section we are going to discuss briefly some of other methods also used in this work.

2.4 CASSCF/CASPT2 Theory

This section introduces a brief description of the multiconfigurational methods called Complete Active Space Self-Consistent Field (CASSCF) and Multiconfigurational Second-Order Perturbation Theory (CASPT2). The terminology multiconfigurational refers to methods based on the Multiconfigurational Self-Consistent Field (MCSCF) for wave function optimization.

The electronic correlation can be split in two types: non-dynamical correlation, also called near-degeneracy effects, and dynamical correlation [30]. The CASSCF method is recommend to treat non-dynamical correlation and dynamical correlation is treated by the CASPT2 method, which uses CASSCF plus a second order perturbation theory.

2.4.1 Configuration Interaction Method

Since the Fock operator has an infinite number of eigenvalues and eigenvectors, in practice computational softwares only calculate a finite subset to characterize the ground state. We populate the eigenvectors with two electrons of opposite spin following the energetic order, defining the occupied orbitals. On the other hand, non-occupied ones are called virtual orbitals. Then, the electronic wave function is obtained throught a single Slater determinant build with the occupied spin-orbitals, denoted by $|\phi_0\rangle$.

The Configuration Interaction (CI) method constructs an electronic wave function as a linear combination of Slater determinants with virtual and occupied spin-orbitals:

$$|\phi\rangle = C_0 |\phi_0\rangle + \sum_{a,r} C_a^r |\phi_a^r\rangle + \sum_{a,b,r,s} C_{ab}^{rs} |\phi_{ab}^{rs}\rangle + \sum_{a,b,c,r,s,t} C_{abc}^{rst} \left|\phi_{abc}^{rst}\right\rangle + ... \tag{2.48}$$

The first sum includes determinant states $|\phi_a^r\rangle$ in which an electron is promoted from the occupied spin-orbital $|\psi_a\rangle$ to the virtual one $|\psi_r\rangle$ and are called singly excited; the second term is associated to determinant states $|\phi_{ab}^{rs}\rangle$ in which two occupied spin-orbitals $|\psi_a\rangle$,$|\psi_b\rangle$ are substituted by virtual ones $|\psi_r\rangle$,$|\psi_s\rangle$ and are called doubly

excited; and so on. Remember that $|\psi\rangle$ is given by Eq 2.17.

The problem is solved by diagonalizing the Hamiltonian matrix represented in the basis given in Eq. 2.48. The CI ground-state energy is obtained as the lowest eigenvalue of the CI matrix, and the corresponding eigenvector contains the C's coefficients in Eq. 2.48. The second lowest eigenvalue corresponds to the first excited state, etc. The method is formally exact, in the case of a complete set of spin orbitals and all possible excitations are accounted for. However, the expansion and excitations number must be truncated in practice. The number of possible excited Slater determinants is thus a combinatorial problem, scaling factorially with the number of electrons and basis functions [30].

2.4.2 Multiconfigurational Self-Consistent Field

The MCSCF method is an extension of the CI method since it uses an expansion similar to that in Eq. 2.48, although concomitantly optimizing, in the SCF procedure, the molecular-orbitals and the CI expansion [31]. First of all let us rewrite Eq. 2.48 as

$$|\phi\rangle = \sum_n T_n |\phi_n\rangle , \tag{2.49}$$

where $|\phi_0\rangle$ is the ground state and each element $|\phi_n\rangle$ for $n = 1, 2, ...$ represents a excited state in Eq. 2.48 as $|\phi_1\rangle = \sum_{a,r} C_a^r |\phi_a^r\rangle$, $|\phi_2\rangle = \sum_{a,b,r,s} C_{a,b}^{r,s} |\phi_{a,b}^{r,s}\rangle$, and so on, and T_n stands for the weights of each state.

The electronic energy is given by a functional of the system wave function, i.e., a function of the CI coefficients T_n and the molecular-orbital coefficients C_i,

$$E[\phi_i, C_i, T_i] = \left\langle \sum_n T_n \phi_n \middle| \mathscr{H}_e \middle| \sum_m T_m \phi_m \right\rangle . \tag{2.50}$$

To optimize the wave equation we need to find an energy stationary point. We search for a extremum of Eq 2.50 subjected to the constraints: $\sum_i T_i^2 = 1$ (normalization) and $\langle \phi_i | \phi_j \rangle = \delta_{ij}$ (orthogonality). Employing the Lagrange Multiplicators ϵ, we

obtain

$$\sum_n \langle \phi_m | \mathscr{H}_e | \phi_n \rangle \, T_n - \epsilon \, T_m = 0. \tag{2.51}$$

The electronic energy can be obtained by expanding Eq. 2.50 in a Taylor Series with respect to the variational parameters which we represent by a vector $\mathbf{p} = (\phi_i, C_i.T_i)$ around a $\mathbf{p}_0$ point:

$$E(\mathbf{p}) = E(\mathbf{p}_0) + \sum_i p_i \left(\frac{\partial E}{\partial p_i}\right)_{p_i = p_{0i}} + \frac{1}{2} \sum_{i,j} p_i p_j \left(\frac{\partial E}{\partial p_i \partial p_j}\right)_{p_k = p_{0k}} + ... \tag{2.52}$$

where $k = i, j$. It is interesting to use the matrix notation

$$E(\mathbf{p}) = E(\mathbf{p}_0) + \mathbf{g}^\dagger \mathbf{p} + \frac{1}{2} \mathbf{p}^\dagger \mathbf{H} \mathbf{p} + ..., \tag{2.53}$$

in which $g_i = (\partial E / \partial p_i)_{p_i = p_{0i}}$ is the gradient vector and $H_{ij} = (\partial E / \partial p_i \partial p_j)_{p_k = p_{0k}}$ is an element of the Hessian Matrix $\mathbf{H}$ with $k = i, j$. The stationary points are obtained as solutions of $\partial E / \partial p_i = 0$. We can approximately solve it by truncating Eq. 2.52 in second order, generating the following linear system

$$\mathbf{g} + \mathbf{p}\mathbf{H} = 0 \Longrightarrow \mathbf{p} = -\mathbf{H}^{-1}\mathbf{g}, \tag{2.54}$$

which can be solved using Newton-Raphson method. Then, we can use this solution as a new starting point; new $\mathbf{G}$ and $\mathbf{H}$ are calculated, and Eq. 2.54 is solved again.

The MCSCF can in principle provide highly accurate results, but the computational effort becomes prohibitive in case high-order excitations are accounted for. A cost-effective alternative is provided by the CASSCF/CASPT2 approaches outlined below.

2.4.3 CASSCF and CASPT2

Several types of wave functions can be constructed employing MCSCF formalism and CASSCF is the most widely employed among them. The CASSCF method split orbitals set into four subsets:

1. Core: lowest-energy orbitals with atomic character. They are assumed to remain unchanged during excitation, valence ionization and chemical bond formation;

2. Inactive: orbitals which do not directly participate in process cited above but need to be optimized to improve the description of the electronic system;

3. Active: orbitals which are directly involved the relevant molecular processes and will be optimized;

4. Virtual: virtual orbitals that will remain unoccupied.

The core and inactive orbitals are kept doubly occupied, although the latter are optimized and the first are kept frozen (in the original form generated by an initial SCF calculation). Finally the active orbitals will also be optimized and may be occupied by zero, one or two electrons.

After choosing which orbitals will compose each subset, electrons from active orbitals are distributed in all possible ways in the active orbital subset (full CI in active space), generating all possible configurations which preserve spin and spatial symmetry. Subsequently this configurations are used to define the CASSCF wave function. Since the correlation will only be accounted for the active orbitals, the selection of the active space is the most important part for the calculation.

Finally in order to incorporate electronic dynamical correlation we use CASPT2 method. The idea is to use perturbation theory based on the CASSCF wave function as the zero-th order approximation. In general perturbation methods are based in a decomposition of the Hamiltonian into a zero-th order term that can be solved analytically in principle, and the perturbation. In CASPT2 method the order zero term is chosen to be similar as possible to second-oder Møller-Plesset perturbation theory [30].

2.5 Density Functional Theory

One of the most successful method of electronic structure is the Density Functional Theory (DFT), since it is largely employed for obtain electronic proprieties of macromolecules (over 20 atoms) in general due to its low computational cost [36]. The essence of DFT is the possibility to obtain the desired solution without explicitly calculating the many-body wave function. This theory uses the electronic density $n(\mathbf{r})$ as the fundamental object which only depends on three variables, apart from spin. It is interesting to rewrite the electronic Hamiltonian elements as

$$\mathscr{H}_e = T + V + W, \tag{2.55}$$

in which

$$T = -\sum_{j=1}^{N} \frac{\nabla_j^2}{2},\ V = \sum_{j=1}^{N} v(\mathbf{r}_j) = -\sum_{j,\mu} \frac{Z_\mu}{R_{j\mu}},\ W = \frac{1}{2}\sum_{i\neq j}^{N} w(|\mathbf{r}_j - \mathbf{r}_i|) = \frac{1}{2}\sum_{i\neq j}^{N} \frac{1}{r_{ij}},$$

T, V and W represent the kinetic, external potential (from fix nuclei), and interaction operators (electron-electron repulsion potential), respectively.

DFT is based on two theorems derived by Hohenberg and Kohn [37, 38]. We will consider non-degenerate ground states, and the generalization can be found elsewhere [38]. The electronic density can be written as

$$n(\mathbf{r}) = \langle\psi|\sum_{i=1}^{N} \delta(\mathbf{r} - \mathbf{r}_i)|\psi\rangle, \tag{2.56}$$

$\mathbf{r}$ is a point the three-dimensional space. It will prove useful to express the expectation value of the external potential as follows,

$$\langle\psi|V|\psi\rangle = \int d\mathbf{r}\ n(\mathbf{r})\, v(\mathbf{r}). \tag{2.57}$$

Now we derive the two theorems:

Theorem 1 (KS). *The external potential $V(\boldsymbol{r})$ is a unique functional of the electronic*

density of the ground state $n_0(\boldsymbol{r})$.

Proof. Given a many-body quantum problem

$$\mathscr{H}|\psi_k\rangle = E_k|\psi_k\rangle \tag{2.58}$$

where the Hamiltonian $\mathscr{H}$ is given by Eq. 2.55. Let us consider the sets:

$$\mathscr{V} = \{v| \text{ with: } v \text{ multiplicative, corresponding } |\psi_0\rangle \text{ exists and is non-degenerate, } v'(\mathbf{r}) \neq v(\mathbf{r}) + const\}$$

which represents the set of all external potentials v that generate a non-degenerated ground states as in Eq. 2.58;

$$\mathscr{C} = \{|\psi_0\rangle \,|\, \text{with: } |\psi_0\rangle \text{ ground state corresponding to one element of } \mathscr{V}, \left|\psi_0^{'}\right\rangle \neq e^{i\varphi}|\psi_0\rangle \text{ with } \varphi \text{ being some global phase}\}$$

which represents the set of all ground states $|\psi_0\rangle$ corresponding to only one element of $\mathscr{V}$, and;

$$\mathscr{N} = \{n_0| \; n_0(\mathbf{r}) = \langle\psi_0|n(\mathbf{r})|\psi_0\rangle \text{ and } |\psi_0\rangle \in \mathscr{C}\}$$

which represents the set of all ground electronic densities generated by an element of $\mathscr{C}$. We denoted by A the map from $\mathscr{V}$ to $\mathscr{C}$ and B other map from $\mathscr{C}$ to $\mathscr{N}$. The proof idea is to show that both maps are bijective therefore its composition will also be.

$$A : \mathscr{V} \longrightarrow \mathscr{C}, \quad \mathscr{C} \longrightarrow \mathscr{N}, \quad A \circ B : \mathscr{V} \longrightarrow \mathscr{N}. \tag{2.59}$$

Both maps are well defined because the states are non-degenerated. A and B are also surjective by construction so it is enough to show that both maps are injective.

For the map A, we will derive that a given $|\psi_0\rangle$ state can not be obtained from two different potentials v and v' contained in $\mathscr{V}$. First let us suppose that the above

statement is false:

$$\mathscr{H}\left|\psi_0\right\rangle = \left[T + V + W\right]\left|\psi_0\right\rangle = E_0\left|\psi_0\right\rangle, \tag{2.60a}$$

$$\tag{2.60b}$$

$$\mathscr{H}'\left|\psi_0\right\rangle = \left[T + V' + W\right]\left|\psi_0\right\rangle = E_0'\left|\psi_0\right\rangle. \tag{2.60c}$$

Subtracting the two equation we obtain

$$\left[V - V'\right]\left|\psi_0\right\rangle = \left[E_0 - E_0'\right]\left|\psi_0\right\rangle. \tag{2.61}$$

Therefore

$$\sum_{i=1}^{N}\left[v\left(\mathbf{r}_i\right) - v'\left(\mathbf{r}_i\right)\right] = E_0 - E_0', \tag{2.62}$$

for all points $\mathbf{r}_i$. Keeping $(N-1)$ of the $\mathbf{r}_i$ fixed and letting the remaining position vary, Eq. 2.62 leads to a contradiction, since the right-hand side is constant while v and v' are assumed to differ by more than a constant. Consequently, the map A is unique.

We can employ a similar argument for the map B, starting from two different external potentials $v_1\left(\mathbf{r}\right)$ and $v_2\left(\mathbf{r}\right)$ related to the V_1 and V_2 operators in $\mathscr{V}$. As the energies arising from the two external potentials are distinct, there will be two distinct Hamiltonians and, two different ground electronic states $|\psi_1\rangle$ and $|\psi_2\rangle$. Let us assume that two external potentials generate the same ground electronic density $n_0\left(\mathbf{r}\right)$. From the variational principle:

$$E_1 = \langle\psi_1|\mathscr{H}_1|\psi_1\rangle < \langle\psi_2|\mathscr{H}_1|\psi_2\rangle$$

and

$$E_2 = \langle\psi_2|\mathscr{H}_2|\psi_2\rangle < \langle\psi_1|\mathscr{H}_2|\psi_1\rangle.$$

By subtracting them we obtain

$$\langle\psi_1|\mathscr{H}_1|\psi_1\rangle < \langle\psi_2|\mathscr{H}_2|\psi_2\rangle + \langle\psi_2|V_1 - V_2|\psi_2\rangle \tag{2.63}$$

and

$$\langle\psi_2|\mathscr{H}_2|\psi_2\rangle < \langle\psi_1|\mathscr{H}_1|\psi_1\rangle + \langle\psi_1|V_2 - V_1|\psi_1\rangle\,. \tag{2.64}$$

Using Eq. 2.57

$$E_1 < E_2 + \int d\mathbf{r}\ \left(v_1\left(\mathbf{r}\right) - v_2\left(\mathbf{r}\right)\right) n_0\left(\mathbf{r}\right) \tag{2.65}$$

$$E_2 < E_1 + \int d\mathbf{r}\ \left(v_2\left(\mathbf{r}\right) - v_1\left(\mathbf{r}\right)\right) n_0\left(\mathbf{r}\right). \tag{2.66}$$

Finally summing inequalities above

$$E_1 + E_2 < E_1 + E_2. \tag{2.67}$$

The contradiction arises from the hypothesis that two distinct external potentials $v_1\left(\mathbf{r}\right)$ and $v_2\left(\mathbf{r}\right)$ generate the same electronic density $n_0\left(\mathbf{r}\right)$. One is lead to conclude that the uniqueness of $n_0\left(\mathbf{r}\right)$ requires the uniqueness of the ground state, $|\psi\rangle_1 = |\psi\rangle_2$. □

On other words the electronic density $n_0\left(\mathbf{r}\right)$ contains all the information on the wave function. Every physical observable O has an expectation value given by the unique ground electronic density:

$$\langle O\rangle = \langle\psi\left[n_0\left(\mathbf{r}\right)\right]|O|\psi\left[n_0\left(\mathbf{r}\right)\right]\rangle = O\left[n_0\left(\mathbf{r}\right)\right]. \tag{2.68}$$

Theorem 2 (KS)**.** *The ground state energy $E\left[n_0\right]$ has an absolute minimum at the exact electronic ground density $n_0\left(\boldsymbol{r}\right)$.*

Proof. The functional $E[n_0]$ can be written as

$$E[n_0] = \langle\psi_0|\mathscr{H}|\psi_0\rangle \tag{2.69a}$$

$$= \langle\psi_0|T+W|\psi_0\rangle + \langle\psi_0|V|\psi_0\rangle \tag{2.69b}$$

$$\equiv F[n_0] + \langle\psi_0|V|\psi_0\rangle\,. \tag{2.69c}$$

in which $|\psi_0\rangle$ is the ground state, and $F[n_0]$ is an universal functional, in the sense that it has the same form for any N electron system regardless of the external potential. As the electronic density is unequivocally determined by the external potential and each density is associated with a single electronic state, we can resort again to the variational principle to conclude that

$$\langle\psi_0|\mathscr{H}|\psi_0\rangle < \langle\psi|\mathscr{H}|\psi\rangle \tag{2.70a}$$

$$F[n_0] + \langle\psi_0|V|\psi_0\rangle < F[n] + \langle\psi|V|\psi\rangle \tag{2.70b}$$

$$E[n_0] < E[n] \tag{2.70c}$$

for $n \neq n_0$. □

This second theorem provides a way to search for the electronic ground state density.

2.5.1 Kohn-Sham Formalism

For a given density n, the universal functional from Eq. 2.69c can be written as

$$F[n] = \frac{1}{2}\int d\mathbf{r}\int d\mathbf{r'}\,\frac{n(\mathbf{r})\,n(\mathbf{r'})}{|\mathbf{r}-\mathbf{r'}|} + G[n]\,, \tag{2.71}$$

where the first term ins the electron-electron Coulomb term, $n(\mathbf{r})$ is a generic density and $G[n]$ is the functional which represent the remaining interactions. In that way

we can obtain the energy as

$$E[n] = \int d\mathbf{r}\; n(\mathbf{r})\, v_0(\mathbf{r}) + \frac{1}{2}\int d\mathbf{r} \int d\mathbf{r'}\; \frac{n(\mathbf{r})\, n(\mathbf{r'})}{|\mathbf{r}-\mathbf{r'}|} + G[n]\,. \tag{2.72}$$

In 1965 Kohn and Sham proposed a strategy to calculate the electron structure based on the above functional. It consist in splitting $G[n]$ in two contributions

$$G[n] = T_s[n] + E_{xc}[n]\,, \tag{2.73}$$

where $T_s[n]$ represents the functional of N non-interacting electrons kinetic energy which have the same electronic density of the interacting system, and $E_{xc}[n]$ stands for the electronic correlation, exchange energy, and correction for kinetic energy (XC). In that way the energy becomes

$$E[n] = \int d\mathbf{r}\; n(\mathbf{r})\, v_0(\mathbf{r}) + \frac{1}{2}\int d\mathbf{r} \int d\mathbf{r'}\; \frac{n(\mathbf{r})\, n(\mathbf{r'})}{|\mathbf{r}-\mathbf{r'}|} + T_s[n] + E_{xc}[n]\,. \tag{2.74}$$

Now we use again the variational principle for the $E[n]$ functional, imposing the constraint

$$\int d\mathbf{r}\; n(\mathbf{r}) = N, \tag{2.75}$$

through Lagrange Multipliers μ

$$\delta\left\{E[n] - \mu\left[\int d\mathbf{r}\; n(\mathbf{r})\right]\right\} = 0 \tag{2.76}$$

such that

$$\int d\mathbf{r}\; \delta n(\mathbf{r})\left\{\frac{\delta T_s}{\delta n_0(\mathbf{r})} + v_0(\mathbf{r}) + \int d\mathbf{r'}\; \frac{n(\mathbf{r'})}{|\mathbf{r}-\mathbf{r'}|} + v_{xc}[n] - \mu\right\} = 0, \tag{2.77}$$

where v_{xc} is given by the functional derivative

$$v_{xc}(\mathbf{r}) = \frac{\delta E_{xc}(\mathbf{r})}{\delta n(\mathbf{r})}. \tag{2.78}$$

Since the electronic density can be defined from an electronic wave function, it is convenient to define one-particle wave functions $\varphi_i(\mathbf{r})$ and the Slater determinant know as KS Determinant:

$$\psi(\mathbf{r}_1, ..., \mathbf{r}_N) = \frac{1}{\sqrt{N!}} \begin{vmatrix} \varphi_i(\mathbf{r}_1) & ... & \varphi_k(\mathbf{r}_1) \\ \varphi_i(\mathbf{r}_2) & ... & \varphi_k(\mathbf{r}_2) \\ \vdots & \ddots & \vdots \\ \varphi_i(\mathbf{r}_N) & ... & \varphi_k(\mathbf{r}_N) \end{vmatrix}, \tag{2.79}$$

in that way $\psi(\mathbf{r}_1, ..., \mathbf{r}_N)$ generates the same density $n(\mathbf{r})$ of the electronic problem. Now we are able to rewrite Eq. 2.77. Starting from the first term which represents kinetic energy:

$$\frac{\delta T_s}{\delta n(\mathbf{r})} = -\frac{1}{2}\frac{\delta}{\delta n}\left\{\sum_i \int d\mathbf{r}\ \varphi_i^*(\mathbf{r})\nabla^2\varphi_i(\mathbf{r})\right\} \tag{2.80}$$

with

$$n(\mathbf{r}) = \sum_i |\varphi_i(\mathbf{r})|^2. \tag{2.81}$$

Using Eqs. 2.80 and 2.81 into Eq. 2.77 we obtain a one-particle Schrödinger equation:

$$\left[-\frac{\nabla^2}{2} + v_s[n](\mathbf{r})\right]\varphi_i(\mathbf{r}) = \epsilon_i\varphi_i(\mathbf{r}), \tag{2.82}$$

in which $v_s[n]$ is called the KS effective potential

$$v_s[n] = v_0(\mathbf{r}) + \int d\mathbf{r'}\ \frac{n(\mathbf{r})}{|\mathbf{r} - \mathbf{r'}|} + v_{xc}[n]. \tag{2.83}$$

For closed shell systems the KS determinant can be built from $N/2$ orbitals since each orbital is populated by two electrons with opposite spins. The electronic density is given by

$$n_0(\mathbf{r}) = 2\sum_{i=1}^{N/2} \left|\varphi_i^{KS}(\mathbf{r})\right|^2, \tag{2.84}$$

and the energy can be calculated as

$$E\left[n_0\right] = 2\sum_{i=1}^{N/2}\epsilon_i - \int d\mathbf{r}\; v_{xc}\left(\mathbf{r}\right) n_0\left(\mathbf{r}\right) - E_H\left[n_0\right] + E_{xc}\left[n_0\right], \tag{2.85}$$

where

$$E_H\left[n_0\right] = \frac{1}{2}\int\int d\mathbf{r}d\mathbf{r'}\;\frac{n_0\left(\mathbf{r}\right) n_0\left(\mathbf{r'}\right)}{\left|\mathbf{r}-\mathbf{r'}\right|}. \tag{2.86}$$

For open shell systems we use spin-polarized KS equations. As in open shell HF equations we also define $n_\uparrow$ for up spin electrons and $n_\downarrow$ for down spin electrons with $n_\uparrow + n_\downarrow = N$. So the electronic density can be written as

$$n\left(\mathbf{r}\right) = n_\uparrow\left(\mathbf{r}\right) + n_\downarrow\left(\mathbf{r}\right) = \sum_{i=1}^{N_\uparrow}\left|\varphi_i^\uparrow\left(\mathbf{r}\right)\right|^2 + \sum_{i=1}^{N_\downarrow}\left|\varphi_i^\downarrow\left(\mathbf{r}\right)\right|^2. \tag{2.87}$$

One thus obtains two sets of KS equations, one for each spin:

$$\left[-\frac{\nabla^2}{2} + v_s^\xi\left[n\right]\left(\mathbf{r}\right)\right]\varphi_i^\xi\left(\mathbf{r}\right) = \epsilon_i^\xi\varphi_i^\xi\left(\mathbf{r}\right), \tag{2.88}$$

where $\xi = \uparrow, \downarrow$ and the effective potential $v_s^\xi\left[n\right]$ is given by:

$$v_s^\xi\left[n\right] = v_0\left(\mathbf{r}\right) + \int d\mathbf{r'}\;\frac{n\left(\mathbf{r'}\right)}{\left|\mathbf{r}-\mathbf{r'}\right|} + \frac{\delta E_{xc}\left[n_\uparrow, n_\downarrow\right]}{\delta n_\xi}. \tag{2.89}$$

Although DFT is formally exact, any practical applications require approximations. The first one is the XC functional $E_{xc}\left[n\right]$ and $v_{xc}\left(\mathbf{r}\right)$ which have only been defined mathematically. Once an approximation to the exchange-correlation density functional is defined, a SCF self-consistency cycle must be performed until convergence is achieved.

2.6 Functionals

In this section we discuss the B3LYP and ωB97XD DFT functionals which were employed in this work. The key difference between many DFT-based approximations

is the choice of functional form for the exchange-correlation energy. It can be shown that the exchange-correlation potential is a unique functional [31], valid for all systems, but the explicit form is not known except for special cases such as an uniform electron gas.

The Local Spin Density Approximation (LSDA) approximates the XC energy in real space point $\mathbf{r}$, as the XC homogeneous electron gas energy of density $n(\mathbf{r})$. In this approximation, it is supposed that the electronic density varies slowly in the vicinity of $\mathbf{r}$, such that

$$\begin{aligned} E_{xc}[n_\uparrow, n_\downarrow] \approx E_{xc}^{LSDA}[n_\uparrow, n_\downarrow] = \int d\mathbf{r} \ \left(\epsilon_x(n_\uparrow(\mathbf{r})) + \epsilon_c(n_\uparrow(\mathbf{r}))\right) n_\uparrow(\mathbf{r}) + \\ + \int d\mathbf{r} \ \left(\epsilon_x(n_\downarrow(\mathbf{r})) + \epsilon_c(n_\downarrow(\mathbf{r}))\right) n_\downarrow(\mathbf{r}). \end{aligned} \tag{2.90}$$

We could write $E_{xc}^{LSDA}[n_\uparrow, n_\downarrow]$ as a sum of two terms:

$$E_{xc}^{LSDA}[n_\uparrow, n_\downarrow] = E_x^{LSDA}[n_\uparrow, n_\downarrow] + E_c^{LSDA}[n_\uparrow, n_\downarrow], \tag{2.91}$$

where

$$E_x^{LSDA}[n_\uparrow, n_\downarrow] = \int d\mathbf{r} \ \left(\epsilon_x(n_\uparrow(\mathbf{r}))\, n_\uparrow(\mathbf{r}) + \epsilon_x(n_\downarrow(\mathbf{r}))\, n_\downarrow(\mathbf{r})\right) \tag{2.92}$$

and

$$E_c^{LSDA}[n_\uparrow, n_\downarrow] = \int d\mathbf{r} \ \left(\epsilon_c(n_\uparrow(\mathbf{r}))\, n_\uparrow(\mathbf{r}) + \epsilon_c(n_\downarrow(\mathbf{r}))\, n_\downarrow(\mathbf{r})\right). \tag{2.93}$$

In the LSDA approximation an analytical expression for Eq. 2.92 can be obtained from the homogeneous quantum electron gas theory:

$$E_x^{LSDA}[n_\uparrow, n_\downarrow] = 2^{1/3} C_x \int d\mathbf{r} \ \left\{(n_\uparrow(\mathbf{r}))^{4/3} + (n_\downarrow(\mathbf{r}))^{4/3}\right\} \tag{2.94}$$

in which

$$C_x = \frac{3}{4}\left(\frac{3}{\pi}\right)^{1/3}. \tag{2.95}$$

On the other hand, since an expression for Eq. 2.93 was not obtained analytically, there are several parameterized propositions that have been calibrated over the years.

One of the most utilized is the Perdew-Zunger parametrization [39].

The Generalized Gradient Approximation (GGA) could be understand as a LSDA refinement, which incorporates in the XC term the gradient of the density in the point $\mathbf{r}$. This approximation is understood as a correction to LSDA because in physical systems, generally, the electronic density is far from uniform. The functional assumes the following form:

$$E_{xc}^{GGA}[n] = \int d\mathbf{r}\ f\left(n\left(\mathbf{r}\right), \nabla n\left(\mathbf{r}\right)\right). \tag{2.96}$$

As in Eq. 2.91 this term can be separated,

$$E_{xc}^{GGA}[n] = E_{x}^{GGA}[n] + E_{c}^{GGA}[n]. \tag{2.97}$$

The following analytical expression is obtained for the exchange term:

$$E_{x}^{GGA}[n] = -\frac{3}{4}\left(\frac{3}{\pi}\right)^{1/3} \int d\mathbf{r}\ \left(n\left(\mathbf{r}\right)\right)^{4/3} F\left(s\left(\mathbf{r}\right)\right) \tag{2.98}$$

where $F\left(s\left(\mathbf{r}\right)\right)$ is a function of the reduced gradient,

$$s\left(\mathbf{r}\right) = \frac{\left|\nabla n\left(\mathbf{r}\right)\right|}{2k_F n\left(\mathbf{r}\right)} \tag{2.99}$$

in which $k_F = \left(3\pi^2 n\right)^{1/3}$.

Note that for $F\left(s\left(\mathbf{r}\right)\right) = 1$ we obtain an exchange functional with the same form as in the LSDA approximation. Similarly to LSDA approximation, there are no analytical expressions for the electron correlation term $E_{c}^{GGA}[n]$, parameterizations can be found in literature [38].

From LSDA and GGA approximations some functionals were built considering combinations between XC functionals base on DFT and HF known as hybrid functionals.

The B3LYP Functional

The B3LYP (Beck, *3-parameter*, Lee-Yang-Parr) [40] is one of the most employed for molecules and macromolecules, because it reasonably describe several physical and chemical properties and has low computational cost. It is given by the following expression

$$\begin{aligned} E_{xc}^{B3LYP}[n] = E_x^{LSDA}[n] + a_0\left(E_x^{HF}[n] - E_x^{LSDA}[n]\right) + \\ + a_x\left(E_x^{GGA}[n] - E_x^{LSDA}[n]\right) + a_c\left(E_c^{GGA}[n] - E_c^{LSDA}[n]\right), \end{aligned} \tag{2.100}$$

in which $a_0 = 0.20$, $a_x = 0.72$ e $a_c = 0.81$.

The ωB97XD Functional

One of the serious shortcomings of standard DFT methods is the inability to describe dispersion forces (part of van der Waals-type interactions) [41]. Many functionals provide a purely repulsive inter action between rare gas atoms, while others describe a weak stabilizing interaction, but fail to have the correct R^{-6} long-range distance behavior [30].

The ωB97XD is a hybrid functional which also takes dispersion effects into account [42]. It incorporates an empirical atom-atom dispersion potential, at very low computational cost. These DFT-D (density functional theory with empirical dispersion corrections) are generally satisfactory for large set of non-covalent systems [43]. The main idea is to add the dissipation energy to the hybrid GGA functional. In this scheme, the total energy is given by

$$E_{\text{DFT-D}} = E_{\text{DFT}} + E_{\text{disp}}, \tag{2.101}$$

in which E_{DFT} stand for the DFT energy calculated with ωB97X functional [44] and E_{disp} represents an empirical atomic-pairwise dispersion correction, given by

$$E_{\text{disp}} = -\sum_{i=1}^{N_{\text{at}}-1}\sum_{j=i+1}^{N_{\text{at}}}\frac{C_6^{ij}}{R_{ij}^6} f_{\text{damp}}(R_i j), \tag{2.102}$$

where N_{at} is the number of atoms in the system, C_6^{ij} is the dispersion coefficient for atom pair ij, and R_{ij} is an inter-atomic distance. The model for f_{damp} function is motivated by the conditions of zero dispersion correction at short inter-atomic separations and the correct asymptotic pairwise van der Waals potentials. It is written as

$$f_{\text{damp}}\left(R_{ij}\right) = \frac{1}{1 + a\left(R_{ij}/R_r\right)^{-12}}, \tag{2.103}$$

which reduces to one at large R_{ij}, while vanishing fast enough to prevent divergence of the undamped van der Waals potentials at small R_{ij}. The R_r is the sum of van der Waals radii of the atomic pair ij [45], and the only non-linear parameter, a, controls the strength of dispersion corrections.

Chapter 3

Theoretical Methods II: Transient States

This chapter is dedicated to discuss the theoretical methodology utilized to solve the electron-molecule collision for low energies (< 12eV). We introduce the theoretical framework of a general scattering problem, the Schwinger Multichannel Method, outlining its relevant points. The collision energies of interest lie in the range 0-10 eV, safely below the relativistic regime. Only Coulomb interactions ($\propto 1/r$) are considered and thus, spin-dependent interactions and fine structure terms are neglected, and the fixed-nuclei approximation is also employed. We also briefly address resonances and dissociation induced by electron attachment.

3.1 Electron-Molecule Scattering: General Aspects

We consider an electron beam with a well defined incident wave vector, $\mathbf{k}_i$, colliding against a molecular target with M nuclei and N electrons. The nuclei are held fixed, neglecting the vibrational and rotational degrees of freedom, and ionization is also disregarded. If we denote by V the projectile-target interaction potential operator, the scattering Hamiltonian has the form of

$$\mathscr{H} = T_{N+1} + \mathscr{H}_e + V, \tag{3.1}$$

in which T_{N+1} and $\mathscr{H}_e$ are the incident electron kinetic energy and the electronic Hamiltonian of the isolated molecule (Eq. 2.6), respectively. The potential operator is given (in atomic units) by

$$V = -\sum_{A=1}^{M} \frac{Z_A}{|\mathbf{r}_{N+1} - \mathbf{R}_A|} + \sum_{j=1}^{N} \frac{1}{|\mathbf{r}_{N+1} - \mathbf{r}_j|}, \tag{3.2}$$

where $\{\mathbf{r}_j\}$ and $\{\mathbf{R}_A\}$ are the electronic and nuclear coordinates, respectively.

The final states of the system define the collision channels. In the present formulation, we only consider elastic scattering and electronic excitation channels. Energy conservation imposes

$$E = \frac{k_{\Gamma^i}^2}{2} + \epsilon_{\Gamma^i} = \frac{k_{\Gamma^f}^2}{2} + \epsilon_{\Gamma^f}, \tag{3.3}$$

where $\Gamma^i(\Gamma^f)$ denotes systems initial (final) state, $k_{\Gamma^i}(k_{\Gamma^f})$ is the incident (scattered) electron linear moment, $\epsilon_{\Gamma^i}(\epsilon_{\Gamma^f})$ is the initial (final) target electronic energy, and E is the constant system energy. Energetically accessible channels which respect Eq. 3.3 are said to be open, and those violating energy conservation are said to be closed.

The solutions are eigenstates of $\mathscr{H}$ with the appropriate boundary condition,

$$\mathscr{H}\ \Psi_{\mathbf{k}\Gamma^i}\left(\mathbf{r}_1, ..., \mathbf{r}_{N+1}\right) = E\ \Psi_{\mathbf{k}\Gamma^i}\left(\mathbf{r}_1, ..., \mathbf{r}_{N+1}\right), \tag{3.4}$$

with

$$r_{N+1} \to \infty \Longrightarrow \Psi_{\mathbf{k}\Gamma_i}\left(\mathbf{r}_1, ..., \mathbf{r}_{N+1}\right) \to S_{\Gamma^i} + \sum_{\Gamma^f}^{open} f_{\Gamma^i,\Gamma^f} \Phi_{\Gamma^f} \otimes \frac{\exp\{i\mathbf{k}_f \cdot \mathbf{r}_{N+1}\}}{r_{N+1}}, \tag{3.5}$$

the target is assumed a closed-shell molecule and the spin states are omitted for simplicity, and S_{Γ^i} is the interaction free solution which satisfies

$$\left(T_{N+1} + \mathscr{H}_e\right) |S_{\Gamma^i}\mathbf{k}_{\Gamma^i}\rangle = \left(\epsilon_{\Gamma^i} + \frac{k_{\Gamma^i}^2}{2}\right) |S_{\Gamma^i}\mathbf{k}_{\Gamma^i}\rangle\,. \tag{3.6}$$

Where $|S_{\Gamma^i}\mathbf{k}_{\Gamma^i}\rangle = |\Phi_{\Gamma^i}\rangle \otimes |\mathbf{k}_{\Gamma^i}\rangle$. Each sum element in Eq. 3.5 refers in a spherical wave associated to a Γ^f state. The scattering amplitudes that modulate the amplitude of

the spherical waves $f\left(\mathbf{k}_{\Gamma^i}, \mathbf{k}_{\Gamma^f}\right)$ contain all the relevant scattering information and, therefore, are the central objects of theoretical methods. It is worth mentioning that the boundary condition given by Eq. 3.5 excludes the ionization channels [9].

3.1.1 Lippmann-Schwinger Equation

It is possible to incorporate the Eq. 3.5 boundary conditions through a Green's function. In order to do this we rewrite Eq. 3.1 Hamiltonian as:

$$\mathscr{H} = \mathscr{H}_0 + V, \tag{3.7}$$

where

$$\mathscr{H}_0 = T_{N+1} + \mathscr{H}_e. \tag{3.8}$$

Such that $\mathscr{H}_0 \ |S_{\Gamma^i}\rangle = \left(\epsilon_{\Gamma^i} + \frac{k_{\Gamma^i}}{2}\right) \ |S_{\Gamma^i}\rangle$. The general solution will be composed of the homogeneous ($|S_{\Gamma^i}\rangle$) and a particular solution which can be obtained by the Green's function method:

$$\left|\Psi^{(\pm)}_{\Gamma^i}\right\rangle_P = G_0^{(\pm)} V \left|\Psi^{(\pm)}_{\Gamma^i}\right\rangle_P, \tag{3.9}$$

where (+) and (-) stand for the boundary conditions built on outgoing and incoming spherical waves, respectively [9]. The The Green's operator associated with $\mathscr{H}_0$ can be expressed as

$$G_0^{(\pm)} = \lim_{\epsilon \to 0} \frac{I}{E - \mathscr{H}_0 \pm i\epsilon}, \tag{3.10}$$

where the identity operator is written as

$$I = 1_N \otimes 1_{\mathbf{k}} = \sum\!\!\!\!\!\!\int_{\Gamma^i} d^3k \ \left|\Phi_{\Gamma^i}\mathbf{k}\right\rangle \left\langle \mathbf{k}\Phi_{\Gamma^i}\right|, \tag{3.11}$$

where $\sum\!\!\!\!\!\!\int$ symbol denotes a sum over the target discrete bound states and an integration over the continuum spectrum. By the energy conservation, expressed in Eq. 3.3,

the Green's operator will be given by:

$$G_0^{(\pm)} = \lim_{\epsilon \to 0} \sum\!\!\!\!\!\!\int d^3k \, \frac{|\Phi_{\Gamma^i}\mathbf{k}\rangle \langle \mathbf{k}\Phi_{\Gamma^i}|}{\frac{k_{\Gamma^i}^2}{2} - \frac{k^2}{2} \pm i\epsilon}. \tag{3.12}$$

In that way, the scattering state can be obtained as

$$\left|\Psi_{\Gamma^i}^{(\pm)}\right\rangle = |S_{\Gamma^i}\rangle + G_0^{(\pm)} V \left|\Psi_{\Gamma^i}^{(\pm)}\right\rangle, \tag{3.13}$$

know as the Lippmann-Schwinger Equation which is equivalent to Eq. 3.4 with Eq. 3.5 boundary conditions. It is known from the scattering theory [9] that the scattering amplitude can be obtained from Eq. 3.13 and written in different ways:

$$f = -\frac{1}{2\pi} \left\langle S_{\Gamma^f} \middle| V \middle| \Psi_{\Gamma^i}^{(+)} \right\rangle \tag{3.14}$$

and

$$f = -\frac{1}{2\pi} \left\langle \Psi_{\Gamma^f}^{(-)} \middle| V \middle| S_{\Gamma^i} \right\rangle, \tag{3.15}$$

corresponding to different boundary conditions associated with outgoing (+) and incoming (-) boundary conditions.

The scattering amplitude, once obtained, can be used to determinate the differential cross section, which is proportional to its square module, and consequently to obtain the total cross section due a angular integration, as show in Eq. 3.16.

$$\sigma\left(k_{\Gamma^i}, k_{\Gamma^f}\right) = \int d\hat{\mathbf{k}}_{\Gamma^f} \, \frac{d\sigma^{(\text{lab})}}{d\Omega}\left(k_{\Gamma^i}, k_{\Gamma^f}\right) = \int d\hat{\mathbf{k}}_{\Gamma^f} \, \frac{d\sigma^{(\text{body})}}{d\Omega}\left(k_{\Gamma^i}, k_{\Gamma^f}\right), \tag{3.16}$$

where σ, $d\sigma^{(\text{lab})}/d\Omega$ and $d\sigma^{(\text{body})}/d\Omega$ stand for the total cross section and the differential cross section in the laboratory and body frame, respectively. Usually the scattering amplitude is obtained at the body frame and thus the differential cross section too, as opposed to what is experimentally accessed. Experimental scattering measurements are made in a laboratory frame in which z axis is often adopted coinciding with the incident beam. It is possible to make a rotation between body frame

to laboratory frame scattering amplitude by using spherical harmonics and Wigner matrices. Nevertheless, if we are only interested in the integral cross section instead of differential cross section, this transformation is not necessary once the angular integration is rotational invariant. In other words the integral cross section is the same in both frames.

3.2 Schwinger Multichannel Method

The scattering amplitudes calculations are made by Schwinger Multichannel Method (SMC) [46, 47] which is a version of the Schwinger Variational Principle for the scattering amplitude suitable for computational implementation. The method main advantage is the use of square-integrable functions (L^2 type functions) in particular Gaussian-Cartesian functions. We present SMC theoretical below.

Multiplying Eq. 3.13 by the V operator one obtains

$$A^{(\pm)} \left|\Psi_{\Gamma}^{(\pm)}\right\rangle = V \left|S_{\Gamma}\right\rangle , \tag{3.17}$$

in which the $A^{(\pm)}$ operator is

$$A^{(\pm)} = V + VG_0^{(\pm)}V. \tag{3.18}$$

We can use Eqs. 3.15 and 3.17 to obtain a scattering amplitude third expression:

$$f = -\frac{1}{2\pi} \left\langle \Psi_{\Gamma f}^{(-)} \middle| A^{(+)} \middle| \Psi_{\Gamma i}^{(+)} \right\rangle . \tag{3.19}$$

Adding Eqs. 3.14 and 3.15 and subtracting Eq. 3.19 we obtain f as a bilinear form in $\Psi^{(+)}$ and $\Psi^{(-)}$:

$$f = -\frac{1}{2\pi} \left[\left\langle S_{\Gamma f} \middle| V \middle| \Psi_{\Gamma i}^{(+)} \right\rangle + \left\langle \Psi_{\Gamma f}^{(-)} \middle| V \middle| S_{\Gamma i} \right\rangle - \left\langle \Psi_{\Gamma f}^{(-)} \middle| A^{(+)} \middle| \Psi_{\Gamma i}^{(+)} \right\rangle \right] . \tag{3.20}$$

The idea is to use Schwinger Variational Principle in Eq. 3.20. When we perform ar-

bitrary first order variations $\left\langle \Psi_{\Gamma f}^{(-)} \right| \rightarrow \left\langle \Psi_{\Gamma f}^{(-)} + \delta\Psi_{\Gamma f}^{(-)} \right|$ and $\left| \Psi_{\Gamma^i}^{(+)} \right\rangle \rightarrow \left| \Psi_{\Gamma^i}^{(+)} + \delta\Psi_{\Gamma^i}^{(+)} \right\rangle$ we want that Eq. 3.20 amplitude remain stable, $[\delta f] = 0$. This is satisfied if [46, 47]

$$\left(A^{(+)}\right)^{\dagger} = A^{(-)}. \tag{3.21}$$

We can expand Ψ on a trial basis as

$$\left| \Psi_{\Gamma^i}^{(+)} \right\rangle = \sum_{\mu} c_{\mu}^{(+)} \left(\mathbf{k}_i\right) \left|\chi_{\mu}\right\rangle \tag{3.22}$$

and

$$\left\langle \Psi_{\Gamma f}^{(-)} \right| = \sum_{\nu} c_{\nu}^{(-)*} \left(\mathbf{k}_f\right) \left\langle\chi_{\nu}\right| . \tag{3.23}$$

Using stability conditions in f

$$\frac{\delta f}{\delta c_{\mu}^{(+)}} = \frac{\delta f}{\delta c_{\nu}^{(-)*}} = 0, \tag{3.24}$$

We obtain an expression for f:

$$f\left(\mathbf{k}_i, \mathbf{k}_j\right) = -\frac{1}{2\pi} \sum_{\mu,\nu} \left\langle S_{\Gamma f}|V|\chi_{\mu}\right\rangle \left(d^{-1}\right)_{\mu\nu} \left\langle\chi_{\nu}|V|S_{\Gamma^i}\right\rangle , \tag{3.25}$$

where d^{-1} is the inverse of

$$d_{\mu\nu} = \left\langle\chi_{\mu}|A^{(+)}|\chi_{\nu}\right\rangle . \tag{3.26}$$

Since the target is a neutral system, the V interaction potential between the incident electron and the target is short-ranged, making the behavior of the $\{\chi_{\mu}\}$ functions over long distances unimportant for the integrals in Eq. 3.25. This allows us to use square-integrable functions (L_2), as Gaussian-Cartesian functions, to build the set $\{\chi_{\mu}\}$ which is very convenient from the computational point of view. However, the problem is still numerically unfeasible since the representation of the Green's function, as in in Eq. 3.26, involves both the discrete and continuum (ionization) spectra of the target molecule. To overcome this difficulty, we can truncate the representation of the Green's function by introducing a projector onto the energetically open target

states,

$$P \equiv \sum_{l}^{open} \left|\Phi_l\left(\mathbf{r}_1, ..., \mathbf{r}_N\right)\right\rangle \left\langle\Phi_l\left(\mathbf{r}_1, ..., \mathbf{r}_N\right)\right| . \tag{3.27}$$

Applying P operator into Eq. 3.12 we obtain

$$G_P^{\pm} = \lim_{\epsilon \to 0} \sum_{l}^{open} \int d^3k \, \frac{\left|\Phi_l \mathbf{k}\right\rangle \left\langle \mathbf{k} \Phi_l\right|}{\frac{k_l^2}{2} - \frac{k^2}{2} \pm i\epsilon}, \tag{3.28}$$

which only accounts for the energetically accessible channels. The $A^{(\pm)}$ operator become

$$A^{(\pm)} = VP + VG_P^{(\pm)}V. \tag{3.29}$$

However the variational condition Eq. 3.21 is no longer satisfied. To recover the information contained in the complementary space $(1-P)$, we rewrite the Schrödinger equation as [46]

$$\left(E - \mathscr{H}\right)\left[aP + (1 - aP)\right]\left|\Psi^{(+)}\right\rangle = 0, \tag{3.30}$$

where a is an arbitrary parameter which will be determined. We then substitute the projected Lippmann-Schwinger equation in the above Schrödinger equation. After some manipulations we obtain a new expression for the $A^{(+)}$ operator:

$$A_P^{(+)} = \frac{1}{2}\left(PV + VP\right) - VG_P^{(+)} + \frac{1}{a}\left[\hat{H} - \frac{a}{2}\left(\hat{H}P + P\hat{H}\right)\right], \tag{3.31}$$

in which $\hat{H} = E - \mathscr{H}$. The stability conditions given by Eq. 3.21 are satisfied for any $a \, \epsilon \, \mathbb{C}$. In principle, the trial basis $\{\chi_\mu\}$ comprises discrete and continuum functions. The stability condition in Eq. 3.21 would not be satisfied for the matrix elements of the operator A involving two continuum functions. It can be shown that the contribution from these continuum-continuum matrix elements can be zeroed out by the choice $a = (N + 1)$ [46, 47].

The final expression of the scattering amplitude is given by

$$f\left(\mathbf{k}_i, \mathbf{k}_j\right) = -\frac{1}{2\pi} \sum_{\mu,\nu} \left\langle S_{\Gamma^f} | V | \chi_\mu \right\rangle \left(d^{-1}\right)_{\mu\nu} \left\langle \chi_\nu | V | S_{\Gamma^i} \right\rangle, \tag{3.32}$$

in which d was modified as follows:

$$d_{\mu\nu} = \langle \chi_\mu | A_P^{(+)} | \chi_\nu \rangle \,. \tag{3.33}$$

Furthermore, it is worth mentioning that at very low energies ($\gtrsim 0$) there are no contributions from electronically inelastic channels, thus only the elastic channel should be considered. The target is assumed to be initially in its ground state and, such that for elastic scattering, $P = |\phi_0\rangle\langle\phi_0|$.

3.3 Implementation and Numerical Procedures

In the SMC method, a significant part of the computational effort is related to the two-electron integrals. The number of integrals scales as N^4, where N is the number of single-particle basis functions (orbitals). For heavier atoms, actually all but hydrogen, the calculation with core electrons can increase the numerical effort considerably. To alleviate this problem we employ the pseudo potentials (PPs) of Bachelet, Hamann e Schlüter (BHS) [48, 49] to describe the atomic nuclei and core electrons. In this way, we can focus on the valence electrons that have more significantly contributions to bound-state and scattering properties. The formula for BHS PP atoms is

$$V_{PP} = V_{core} + V_{ion}, \tag{3.34}$$

wherein

$$V_{core} = -\frac{Z_v}{r} \sum_{i=1}^{2} c_i \mathrm{erf}\left(\rho_i^{1/2} r\right) \tag{3.35}$$

and

$$V_{ion} = \sum_{n=0}^{1} \sum_{j=1}^{3} \sum_{l=0}^{2} A_{njl} r^{2n} e^{-\sigma_{jl} r^2} \sum_{m=-l}^{l} |lm\rangle\langle lm|, \tag{3.36}$$

in which Z_v is the valence charge, A_{njl}, σ_{jl}, ρ_i and c_i are atomic parameters and erf denotes the error function. In that way, all integrals involving electrostatic interaction between the nuclei and valence electrons are replaced by their respective V_{PP} allowing

for an analytical solution. The SMC implementation with BHS PPs (called SMCPP), as well as how to determine the parameters of each atom, are described in Refs. [48, 49].

The Cartesian Gaussian basis functions to be used along with the BHS PPs have been developed [48, 49], and will be referred to as the BHS basis. For hydrogens, a compact basis proposed by *Dunning et al.* was used [50] (the exponents of the basis sets are presented in Cap. 5).

We now turn attention for the matrix elements of the A operator in Eq. 3.31. The integrals of the $VG_P^{(+)}V$ term in the $\{\chi_\mu\}$ basis are the most numerically demanding step of SMC method. We begin by decomposing the Green's operator (Eq. 3.28) into the real and imaginary part [51]:

$$G_P = G_P^{Pr} + G_P^R, \tag{3.37}$$

which correspond to Cauchy Principal Value (Pr) and the residue (R)

$$G_P^{Pr} = \sum_l^{open} \mathscr{P} \int_0^\infty dk \frac{k^2}{(k_l^2 - k^2)/2} \int d\mathbf{k}\ |\phi_l \mathbf{k}\rangle\langle\phi_l \mathbf{k}| \tag{3.38}$$

and

$$G_P^R = i\pi \sum_l^{open} k_l \int d\mathbf{k}\ |\phi_l \mathbf{k}\rangle\langle\phi_l \mathbf{k}|, \tag{3.39}$$

where $\mathscr{P}$ indicates the Cauchy Principal Value. The matrix elements involved can be decomposed as

$$\langle\chi_\mu|VG_PV|\chi_\nu\rangle = \langle\chi_\mu|VG_P^{Pr}V|\chi_\nu\rangle + \langle\chi_\mu|VG_P^RV|\chi_\nu\rangle, \tag{3.40}$$

thus defining the *off-shell*

$$\langle\chi_\mu|V\mathscr{G}_P^{Pr}V|\chi_\nu\rangle = \sum_l^{open} \mathscr{P} \int_0^\infty dk\ \frac{k^2}{(k_l^2 - k^2)/2} g_{\mu\nu}^l(k) \tag{3.41}$$

and *on-shell* integrals/matrix elements

$$\langle\chi_\mu|VG_P^RV|\chi_\nu\rangle = i\pi\sum_l^{open} k_l g^l_{\mu\nu}(k_l), \tag{3.42}$$

with

$$g^l_{\mu\nu}(k) = \int d\hat{\mathbf{k}}\ \langle\chi_\mu|V|\phi_l\mathbf{k}\rangle\langle\phi_l\mathbf{k}|V|\chi_\nu\rangle. \tag{3.43}$$

As the SMC method allows the use of square-integrable functions to expand the scattering wave function, we deal with some integrals that can be solved analytically, such as those also found in electronic-structure methods. Some integrals that can not be solved analytically, such as the $\mathbf{k}$ integrals which involve plane waves, are solved numerically using the Gauss-Legendre quadrature [52].

3.4 Static-Exchange and Static-Exchange plus Polarization Approximations

The scattering wave function is represented in a $(N+1)$ particle basis and each basis vector $|\chi_\mu\rangle$ is a configuration state function (CSFs), i.e., spin-adapted Slater determinants. Since the SMC is a variational method, a larger CSF space allows for more flexibility. The CSFs are given by an antisymmetric products of target states by scattering orbitals. In this work, we only consider elastic scattering, although we employ two approximations to build the CSF space: Static-Exchange (SE) and Static-Exchange plus Polarization (SEP).

In the SE approximation the molecular target is kept frozen in the ground state $|\Phi_0\rangle$ and its virtual orbitals constitute the scattering orbitals $|\phi_m\rangle$, as

$$|\chi_m\rangle = A_{N+1}\,|\Phi_0\rangle \otimes |\phi_m\rangle\,, \tag{3.44}$$

where A_{N+1} is an anti-symmetrizer operator. The target ground state is described with the HF approximation. This approximation does not allow for the response of the

target electrons to the incoming electron, i.e., the electronic cloud. For collisions with energy above ≈ 20 eV, the SE approach is reasonable. For lower energies, however, the dynamical response of the target electrons, referred to as correlation-polarization effects, has to be accounted for.

In the SEP approximation virtual excitations of the target are allowed, so the CFS space is augmented with configurations of the kind

$$|\chi_{im}\rangle = A_{N+1} |\Phi_i\rangle \otimes |\phi_m\rangle \,, \tag{3.45}$$

in which $|\Phi_i\rangle$ represents a singly excited target state and $|\phi_m\rangle$ a scattering orbital. In this approximation, the virtual excitations account for long-range polarization (induced dipole moment) and short-range correlation.

The SEP functions requires the choice of three orbitals, two of which are associated with the excitation of the target (hole and particle) and the third being the scattering orbital. Since the current implementation is restricted to closed shell targets, the addition of one electron imposes that the global spin is doublet state, and therefore only configurations of this multiplicity of spin are included in the CSF space. The latter space is build according to the energy criterion proposed by Kossoski and Bettega [53]. All single particle orbitals whose energy eigenvalues satisfy $\epsilon_{\text{scat}} + \epsilon_{\text{part}} - \epsilon_{\text{hole}} < \Delta$, where ϵ_{scat}, ϵ_{part}, and ϵ_{hole} are the energies of the scattering, particle, and hole orbitals, respectively, while Δ is a cutoff.

Modified virtual orbitals (MVOs) [54] were used as both particle and scattering orbitals. The MVOs are build by re-optimizing the virtual orbitals in a cationic field, making than more compact than the canonical HF counterparts.

3.5 Resonances Characterization

In electron-molecule interactions, the electron can become temporarily trapped in the vicinity of the molecule, thus forming a TNI. If the system energy is larger than the energy of the isolated molecule in the ground state, it is named a resonance.

Resonances have signatures in the ICS known as Breit-Wigner profiles. These are ideally Lorentzian peaks, which are in practice superimposed by the background (non resonant) contribution to the cross section. In the vicinity of the resonance energy (E_r), the elastic scattering integral cross section approaches a behavior of the form

$$\sigma(E) = \frac{\Gamma^2}{(E - E_r)^2 + (\Gamma/2)^2}, \tag{3.46}$$

where Γ is a resonance auto-ionization width.

In electron-molecule scattering, the resonances are classified in terms of the target states involved in the attachment mechanism. A useful concept is the parentage: a resonance parent state is the state obtained by the exclusion of the incident electron. In a simplified picture, electron attachment process can be associated with temporary occupation of a previously unoccupied MO. Resonances could be energetically above (shape resonace) or bellow (Feshbach resonance) their corresponding parent state. Shape resonances can decay through auto-dissociation. On the other hand, Feshbach resonances are typically long-lived since the auto-aionization of the parent state is a closed channel, i.e., the target must undergo de-excitation along with auto-ionization.

3.5.1 Shape Resonances

The shape resonance is associated with an electron capture in the target ground state. The incident electron populates an empty orbital without any change in the previous electronic structure. In this case, the target ground state is said to be the parent, and the TNI is termed a shape resonance. The shape resonance is observed with energy above that of its parent state, and the decay is an open channel. Fig. 3.1a shows a schematic diagram of this type of resonance.

A shape resonance is described in a qualitatively correct way in the SE approximation, since it does not involve excitation of the molecule, but the energy obtained is overestimated. When described in the SEP approach, the resonance energy decreases, presenting a more accurate value.

3.5.2 Core-Excited Resonances

The core-excited shape resonance is analogous to shape, but is associated with an excited electronic state of the molecule (excited parent state). It could happens when the incoming electron has enough energy to promote one or more electrons from occupied to virtual orbitals. Therefore, this resonance type consists of a hole in one or more occupied orbital(s) and two or more electrons in virtual orbital(s). The core-excited shape resonance is observed with energy above that of its parent state, and the decay is, therefore, an open channel. Fig. 3.1b shows a schematic diagram of this type of resonance.

On the other hand, the Core-Excited Feshbach resonance is observed with energy slightly below than its parent state, therefore presenting a closed channel in relation to auto-ionization. For this type of resonance, the decay in an electronic or vibrational structure is necessary, therefore, its lifetime is considerably longer. Fig. 3.1c shows a schematic diagram of this type of resonance.

3.5.3 Vibrational Feshbach Resonances

While most of the present discussed has been restricted to the fixed-nuclei approximation, it will prove useful to briefly mention vibrationally excited anion states. The incident electron can be trapped in a vibrationally excited anion state known as vibrational Feshbach resonance. It could happens when a shallow anion bound state exists, i.e, an anion state energetically bellow of the neutral ground state (parent state). These kind of anion state are common in strongly polar molecules, which can form bound anion states known as dipole bound states (DBSs) [55]. As show in Fig. 3.1d, the excited states of the anion lie below those of the neutral molecule.

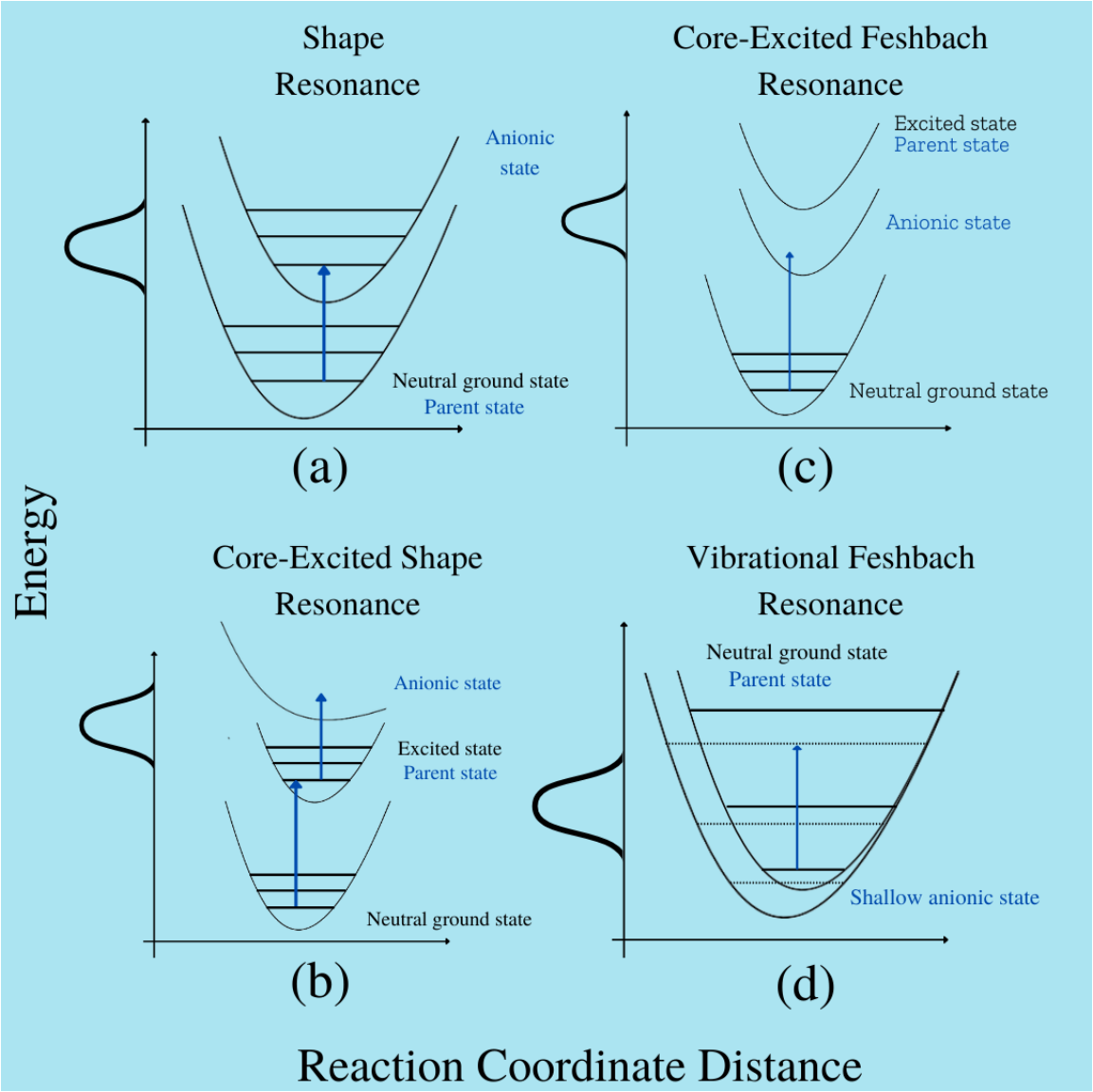

Figure 3.1: A schematic, Born-Oppenheimer, representation of the four common resonances observed in electron scattering. The horizontal normal distribution represent incident electron. The letter states for: a) Shape resonance. b) The core-excited shape resonance. c) Core-excited Feshbach resonance. d) Vibrational Feshbach resonances.

Chapter 4

Bound State Results

This chapter is dedicated to discuss the bound state results for the RS and RV molecules. The description of the target is a necessary preliminary step of the scattering calculations. The molecular geometry optimizations and the electronic structure characterization were performed with the DFT/ωB97XD method and the 6-311++G** basis set [56] for both molecules and its isomers. Another geometry optimization was performed for RV with the B3LYP functional and the same basis set to survey the relevance of dispersion forces.

Finally, we utilized a semi-empirical method, named scaling relation, to explore a well-know correlation between the π^* virtual orbital energies (VOEs) for the neutral species and the vertical attachment energies (VAEs) for the anion states [57]. As a semi-empirical method, it generates different relations for different sets of molecular families. In our case, we utilized Scheer and Burrow DFT relation [58] to estimate the π^* shape resonances energies. The procedure to calculate the VO's is to perform a DFT/B3LYP/6-31G* geometry optimization calculation in the studied molecule. From the obtained VOs, we use the relation

$$\text{VAE} = 0.8065 \times \text{VOE} + 0.9194 \tag{4.1}$$

to determine the correspondent VAEs (in eV). The CASPT2 method with the ANO-L-VDZP basis set [59, 60] were employed to supplement this discussion for the RS molecule.

4.1 Resorcinol

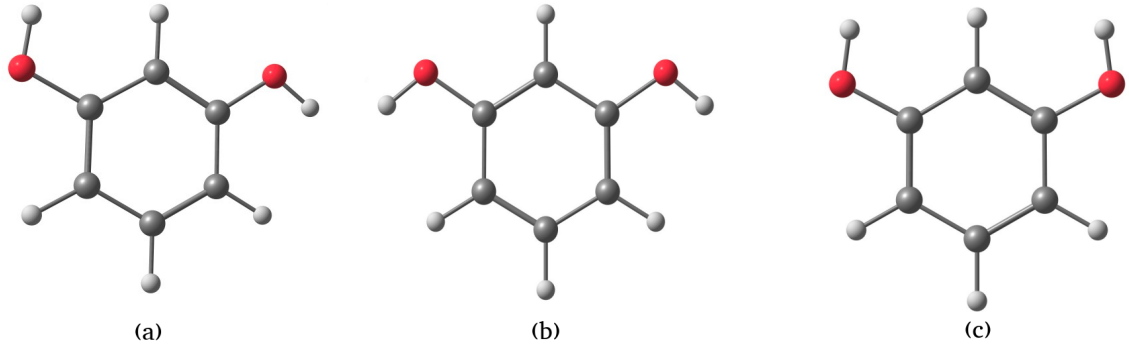

Figure 4.1: Possible geometries of the RS. The colors red, white and grey represent oxygen, hydrogen and carbon atoms respectively.

RS may exist in three possible conformations, brought about by variation in the orientations of the OH groups (labelled A–C in Fig. 4.1). These two conformers, labelled A and B (Fig. 4.1), are nearly iso-energetic, separated only by $\approx$ 1 meV [61]. The geometry of the three conformers, were optimized with the ωB97XD/6-311++G** method, as implemented in *Gaussian09* software [62]. The structures are shown in Fig 4.1 and the relative ground state energies and dipole moments in Tab. 4.1.

Table 4.1: Relative ground state energies ΔE (in eV) and dipole moment magnitudes μ (in Debye) for the three RS conformers shown in Fig. 4.1.

Geo.	ΔE	μ
(a)	0.002	1.4
(b)	0.000	2.5
(c)	0.028	2.3

The three isomers are nearly degenerate, with energy differences between 2 meV and 28 meV, with geometry (b) being the most stable. The thermal energy k_BT at room temperature is $\approx$ 30 meV, such that significant Boltzmann populations would be expected for the three conformations in gas-phase experiments. In contrast, there are relevant differences in the dipole moment magnitudes arising from the orientation of the hydroxyl groups. The dipole moments around 2.0D-2.5D are strong enough to support dipole bound states (DBSs) which can be involved in the formation of vibrational Feshbach resonances, as discussed in Chap. 3. In the following, we focus

on the conformers (a), which breaks the C_{2v} point group symmetry, and (c), which is more likely to form the H_2 molecule through DEA because the hydrogens from hydroxyl group are nearer from eachother.

Both isomers are planar, although the structures (a) and (c) belong to the C_{2v} and C_s symmetry groups, respectively. The vertical electron affinity (VEA), which is a relevant property for electron-molecule interactions, was calculated as the difference between the total energies of the neutral and the anion ground states, at the optimal geometry of the former. We obtained -0.53 eV and -0.69 eV for both (c)- and (a)-RS with CCSD(T)/6-311++G** method, clearly indicating the absence of valence bound states. We also calculated the anion ground state with additional sets of diffuse functions, according to *Skuski et al.* [63], to investigate the possible formation of a DBS. Once more, the calculations did not indicate a bound anion state.

The excitation spectra of the neutral isomers were studied with the CASSCF CASPT2 method and the ANO-L-VTZP basis set, employing the OpenMolcas software [64]. These calculations can indicate the onset of electronic excitation in the scattering calculations and also possible parent states for core-excited resonances. The active space was build with 10 molecular orbitals. In the reference state, the 5 lowest-lying orbitals are doubly occupied and the remaining 5 orbitals are unoccupied. The molecular orbitals and their characters are indicated in Figs. 4.2 and 4.3 for the isomers (c) and (a), respectively.

Tab. 4.2 shows the results for the singlet and triplet of both isomers. At least for the states considered here, the excitation energies are very close for the two conformers, with the lowest triplet states lie around 3.9 eV. For narrow resonances, bound state techniques can provide meaningful energies for resonances [65]. Since we expect narrow π^* resonances for RS and RV, we also performed a CASSCF/CASPT2 study for the anion, although expressing the excitation energies with respect to the ground state of the neutral molecule, for comparison with the resonance energies discussed in Chap. 5. We used the same active space, apart from one additional electron, and could assign two π^* resonances for each isomer, as shown in Tab. 4.2.

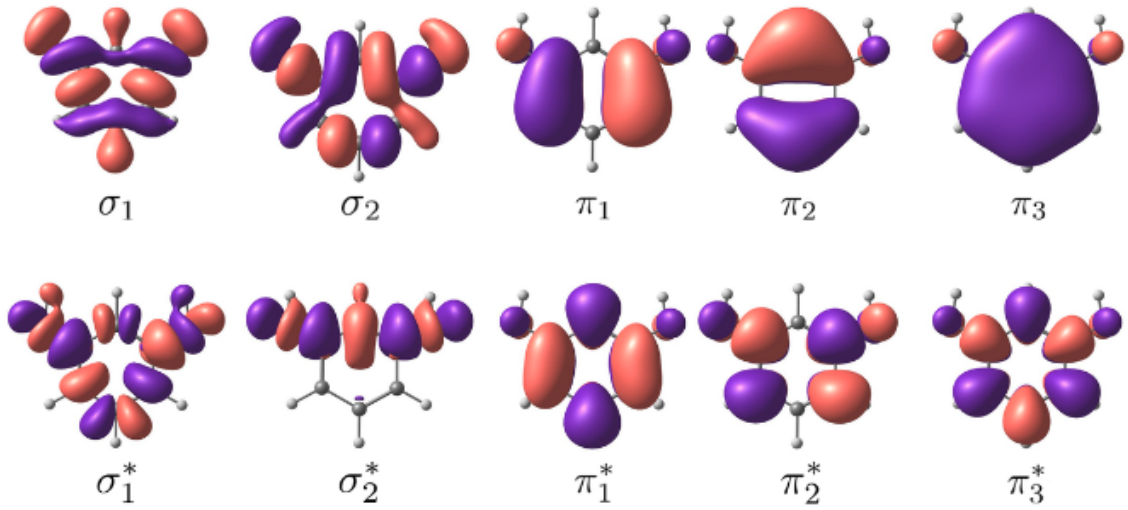

Figure 4.2: Molecular orbitals included in the active space of the CASSCF calculations performed for the (c) isomer of the RS molecule. In the reference state, the five upper orbitals were considered doubly occupied and the five lower orbitals unoccupied.

Table 4.2: Vertical excitation spectra (in eV) for the (c) and (a) isomers of RS obatined with the CASPT2 method. Excitation energies of the anion molecules, expressed with respect to the neutral ground state, are also presented.

		(c)	(a)
Singlet	$1^1\pi\pi^*$	4.43	4.41
	$2^1\pi\pi^*$	5.66	5.47
	$3^1\pi\pi^*$	5.95	5.80
Triplet	$1^3\pi\pi^*$	3.92	3.89
	$2^3\pi\pi^*$	4.02	4.23
	$3^3\pi\pi^*$	4.49	4.42
Anion	$^2\pi_1^*$	1.57	1.49
	$^2\pi_2^*$	2.05	1.97
	$^2\pi_3^*$	-	-

Another simple way to estimate shape resonance energies with bound state techniques is to employ the empirical scaling relations (Eq. 4.1). Based on the three lowest-lying VOEs, shown in Figs. 4.4 and 4.5, one could expect the VAEs shown in Tab. 4.3. The two lowest-lying anion states, labeled π_1^* and π_2^* in order of increasing energy, are consistent with the CASPT2 estimates (Tab. 4.2), although the latter are higher by 0.5 eV. The π_3^* anion (Tab. 4.3) state has a considerably higher energy and was not indicated by the CASPT2 calculations. It is important to observe that the differences between the π^* resonances of the two isomers are always small (< 0.1

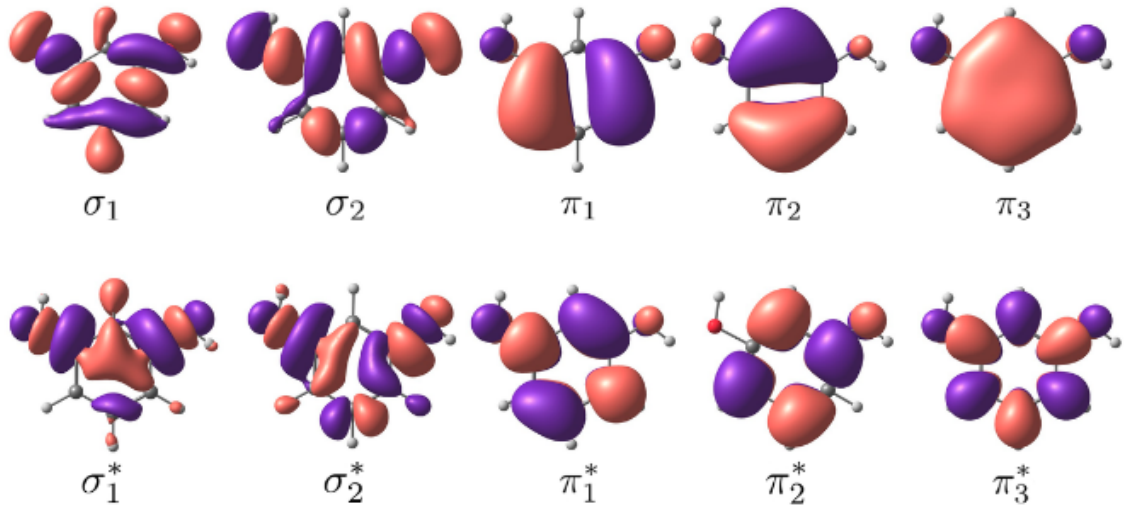

Figure 4.3: Molecular orbitals included in the active space of the CASSCF calculations performed for the (a) isomer of the RS molecule. In the reference state, the five upper orbitals were considered doubly occupied and the five lower orbitals unoccupied.

Table 4.3: Scaled VAE (in eV) obtained from the VOEs (in eV) calculated with compact basis sets, according to Eq. 4.1. The (a) and (c) conformers of RS are indicated by the superscripts.

	VOE^a	VAE^a	VOE^c	VAE^c
π_1^*	0.20	1.08	0.20	1.08
π_2^*	0.63	1.43	0.64	1.44
π_3^*	4.76	4.76	4.77	4.76

eV), according to the CASPT2 and empirical estimates. It will therefore be more convenient to perform the computationally demanding scattering calculations for the (c) conformer, in view of the higher symmetry (C_{2v} group).

4.2 Resveratrol

As stated in the Introduction, RV is the main subject of the present study, RS being one of its subunits. The computational simulations for RV are much more challenging in view of the size, lack of symmetry elements and the existence of *cis* and *trans* isomers. The ground state geometry was optimized with the DFT, employing the B3LYP and ωB97XD functionals and the 6-311++G** basis set, as implemented in *Gaussian09* software [62]. Those frequently used functionals differ in the description

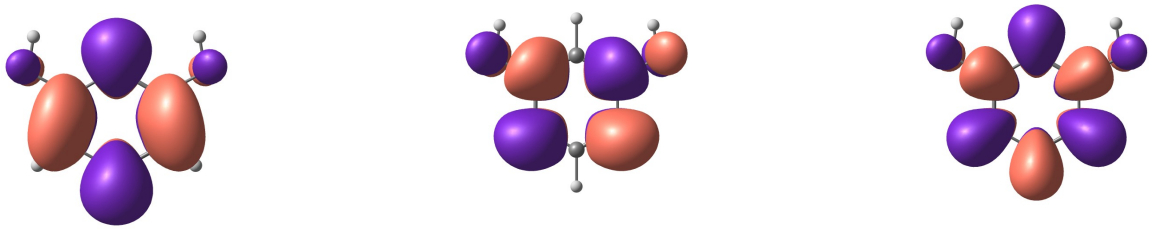

(a) π_1^* (b) π_2^* (c) π_3^*

Figure 4.4: Virtual π^* orbitals for (c)-RS.

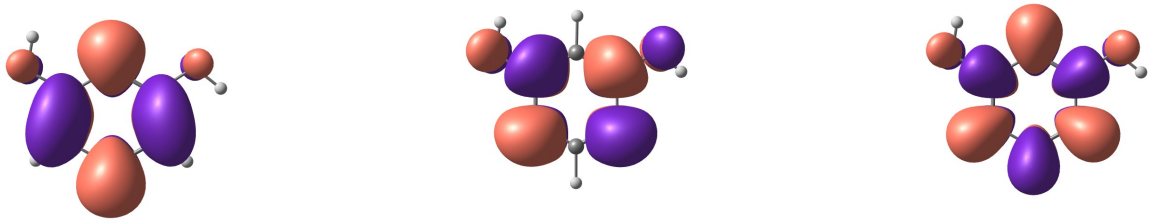

(a) π_1^* (b) π_2^* (c) π_3^*

Figure 4.5: Virtual π^* orbitals for (a)-RS.

of the dispersion (van der Waals) interactions, which are only included in ωB97XD. Since dispersion could be relevant for RV, a molecule with two unsaturated rings [66, 67], the comparison of the two functionals would be interesting.

Since the scattering calculations are computationally expensive, we also considered a planar conformation for *trans*-RV (t-RV), by enforcing the planarity during the geometry optimization. In that way, the use of C_s group symmetry is possible, although the planar geometry does not correspond to a minimum of the potential surface.

The structures of the three isomers optimized with the ωB97XD functional are shown in Fig. 4.6. For the *cis*-RV (c-RV) the geometries obtained with both functionals were similar (Fig. 4.7a). On the other hand, the relative orientation of the two rings in t-RV significantly differ in the two calculations (Fig. 4.7b for ωB97XD and Fig. 4.7c for B3LYP optimized geometries). This is illustrated in Tab. 4.4, where the dihedral angles indicate a nearly planar structure for the B3LYP functional. The labels used in the dihedral angles are defined in Fig. 4.8. As expected, the benzene rings significantly increases the contribution from long-range forces to short-range forces [66, 67] with respect to the optimization calculation. For the planar-RV (p-

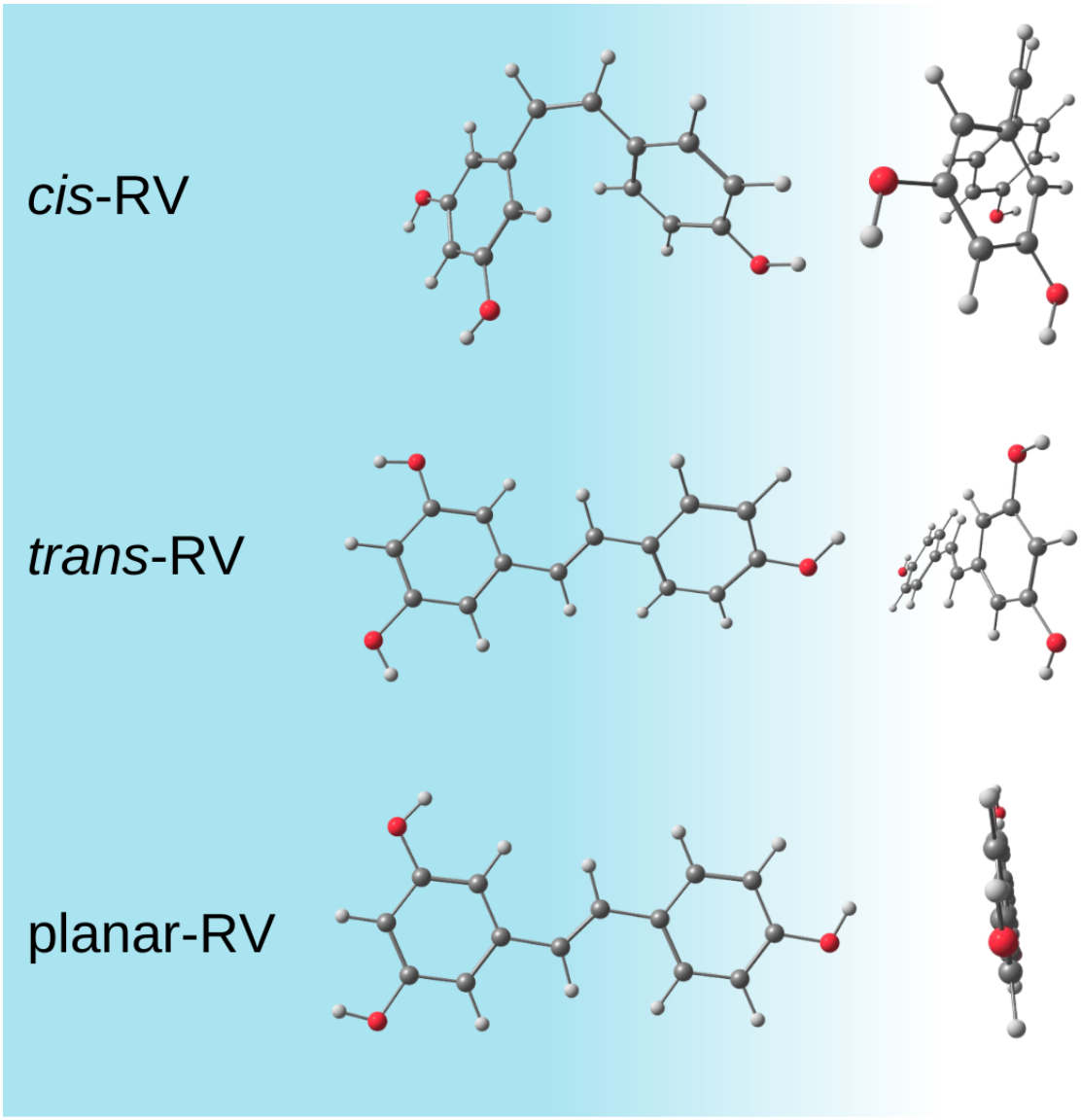

Figure 4.6: Structures of the c- and t-RV isomers, along with the planarized structure, optimized with the ωB97XD method. The oxygen atoms are presented in red, carbon in gray, and hydrogen in white.

RV) the geometries were practically equal (Fig. 4.6).

The relative ground state energies for the three RV structures, calculated with the ωB97XD functional, are shown in Tab. 4.5, along with the dipole moment magnitudes. The t-RV isomer is significantly more stable than the cis counterpart. Under experimental conditions [7], only the trans form has a significant Boltzmann population. It should be clear that the planar form will not be present, despite its low energy, because this conformation is not stable - it is actually a saddle point, see Fig. 4.9. The p-RV structure is considered here to alleviate the computational effort

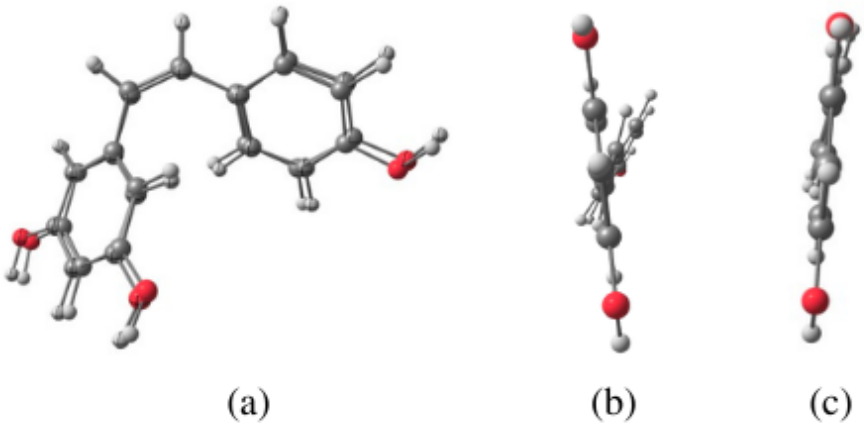

Figure 4.7: (a) Overlap of the two c-RV optimized geometries performed with B3LYP and ωB97XD; (b) t-RV optimized geometry performed with ωB97XD; (c) t-RV optimized geometry performed with B3LYP.

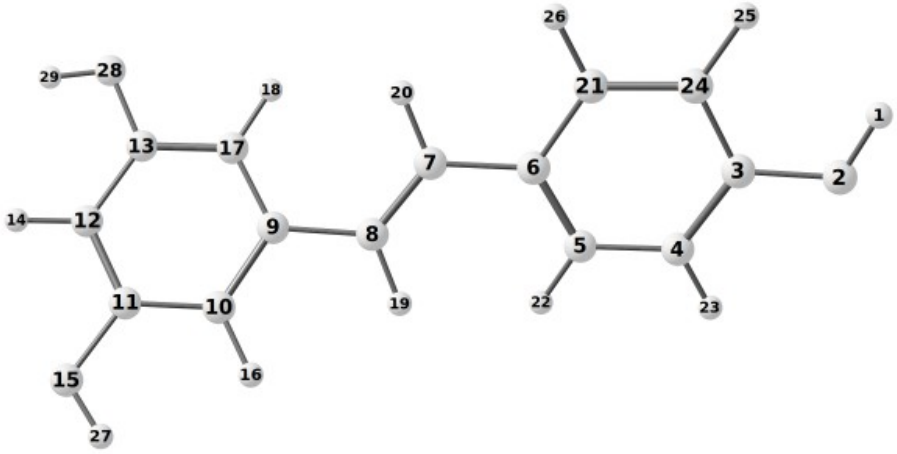

Figure 4.8: Atomic labels used in Tab. 3.5

of the scattering calculations, as already explained.

The t-RV isomer also shows conformers associated with the rotation of the hydroxyl groups. The three conformers shown in Fig. 4.10 differ in energy by 10^{-2} eV and should be present in gas-phase experiments. Despite the nearly degenerate energies, the dipole moment magnitudes vary considerably, from 1.6D to 3.3D. The presence of strongly polar molecules may be important for scattering, as already explained for RS.

We also calculated VEAs for the t- and p-RV isomers, show in Fig. 4.6. The VEA calculated with the ωB97XD functional indicates a shallow bound state, with

Table 4.4: Dihedral angles (in °) for the t-RV isomer calculated with the ωB97XD and B3LYP functionals. The atomic labels are given in Fig. 4.8.

	ωB97XD	B3LYP
5-6-7-8	15.21	4.31
7-8-9-10	159.89	173.86
10-9-8-19	17.88	5.43
5-6-7-20	166.59	176.28

Table 4.5: Ground state energy difference between the most stable one (ΔE) and dipole moment (μ) in relation to RV different geometries.

	ΔE	μ
cis	0.27	1.66
trans	0	1.03
planar	0.01	2.79

binding energy of 30 meV. To confirm this prediction, the VEA was recalculated with several functionals, as shown in Tab. 4.6, with the geometry optimized with the ωB97XD functional. All the functionals confirm the anion bound state, with binding energies from 30 meV to 200 meV. It is therefore reasonable to expect a valence bound state with π^* character and binding energy around $\approx$ 100 meV. The anion bound state orbital character is equivalent to the π_1^* orbital (Fig. 4.11) of the neutral molecule for both t- and p-RV. The DBS existence could not be investigated as RS because of the hardware limitation. However, the RV has a significant number of isomers with compatible dipole moment to form a DBS.

The VAEs were calculated with the empirical scaling relation (Eq. 4.1), as before. However, this correction was calibrated for molecules optimized with the B3LYP/6-31G* method [58]. If we were to re-optimize the t-RV geometry with that functional, the neglect of the dispersion forces would result in a nearly planar structure, as discussed above. We therefore only applied the procedure for the planarized structure. The VAE estimates for the seven lowest-lying π^* orbitals are shown in Tab. 4.7. A shallow valence bound state was also obtained (binding energy of 50 meV), in addition to 6 resonances with energies ranging from 0.9 eV to 5 eV. Due to the molecular size, some of these anion states would lie above the first excited state of the neutral molecule. We estimated the excitation energy of the first triplet state around 2.5 eV

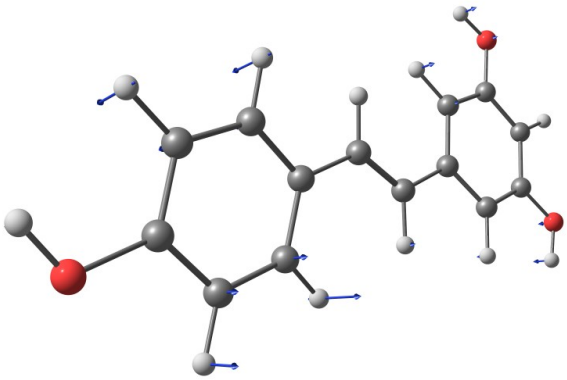

Figure 4.9: Vibrational mode associated with the Imaginary frequency of the planar-RV structure. The vibrational analysis was performed with the ωB97XD functional.

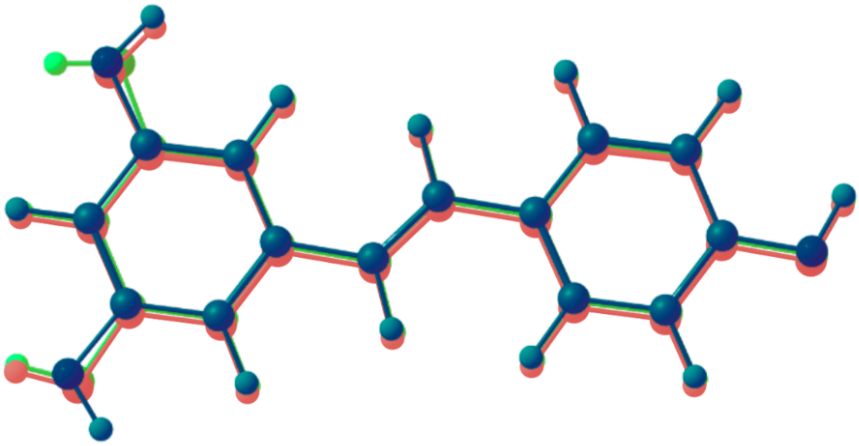

Figure 4.10: Superimposed structures for three conformers of t-RV obtained with the ωB97XD functional, each color stands for a different geometry. Note that geometries differ in the RS subunit.

(2.4 eV) for the t-RV (p-RV) isomer with TDDFT/ωB97XD/6-311++G** method. This result suggests that, if present, the π_5^* to π_7^* could be mixed-character resonances, i.e., admixtures of shape and core-excited resonances.

Finally, we compared compact virtual orbitals, similar to those used in the VAE estimates, for the t- and p-RV isomers. The calculations were performed with ωB97XD/6-31G* and the results are shown in Fig. 4.11. We observe that π_1^*, π_2^*, π_3^* and π_4^* orbitals are very similar for both isomers. While some differences are evident for the higher-lying orbitals.

An interesting observation in Fig. 4.11 is that π_2^* and π_3^* orbitals are localized on the PH and RS subunits, respectively. This result suggest a correlation between some resonances of RV and those of the RS and PH subunits, which is confirmed by

Table 4.6: VEA (eV) and Dipole Moment (D) estimations for RV molecule in its most stable t-geometry (t-RV) and its planar optimized structure (p-RV).

Method	VEA(p-RV)	VEA(t-RV)	μ(p-RV)	μ(t-RV)
B3LYP	0.18	0.11	2.77	1.06
CAMB3LYP	0.11	0.03	2.82	1.05
LC-BLYP	0.11	0.03	2.93	1.06
ωB97XD	0.03	-0.05	2.79	1.03
BP86	0.33	0.27	2.70	1.06
BPBE	0.20	0.14	2.70	1.06
PBEh1PBE	0.17	0.10	2.78	1.06
LC-wPBE	0.13	0.04	2.85	1.08
M05	0.16	0.09	2.79	1.08
M05-2X	0.15	0.07	2.86	1.06
M06-2X	0.15	0.07	2.80	1.04

Table 4.7: The RV scaled VAE (in eV) obtained from the VOEs (in eV) calculated with compact basis sets, according to Eq. 4.1.

	VOE	VAE
π_1^*	-1.20	-0.05
π_2^*	-0.08	0.85
π_3^*	0.67	1.46
π_4^*	0.75	1.53
π_5^*	2.35	2.82
π_6^*	4.75	4.76
π_7^*	5.25	5.15

the comparison of the compact virtual orbitals shown in Fig. 4.12.

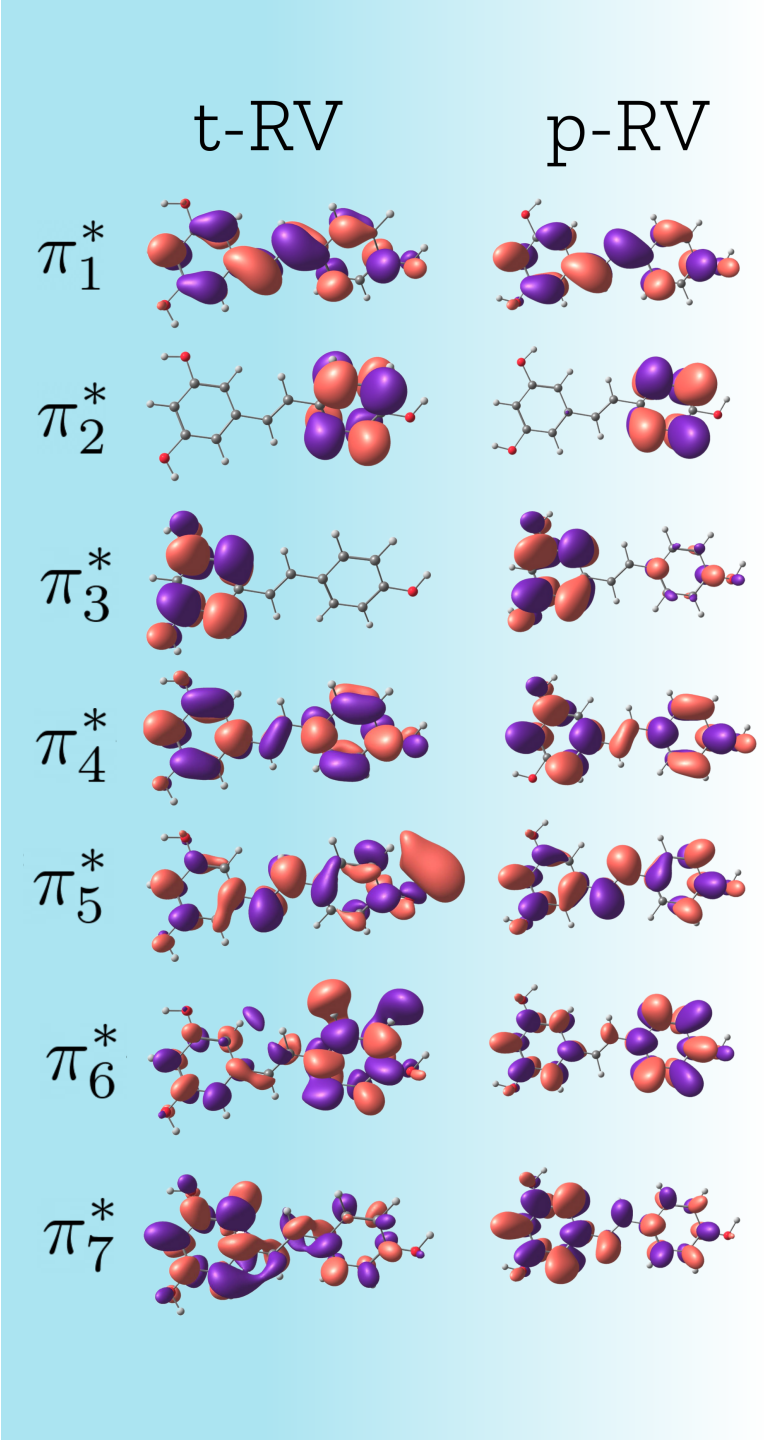

Figure 4.11: $\pi*$ virtual orbitals calculated with the ωB97XD/6-31G* method for t-RV (left) and p-RV (right).

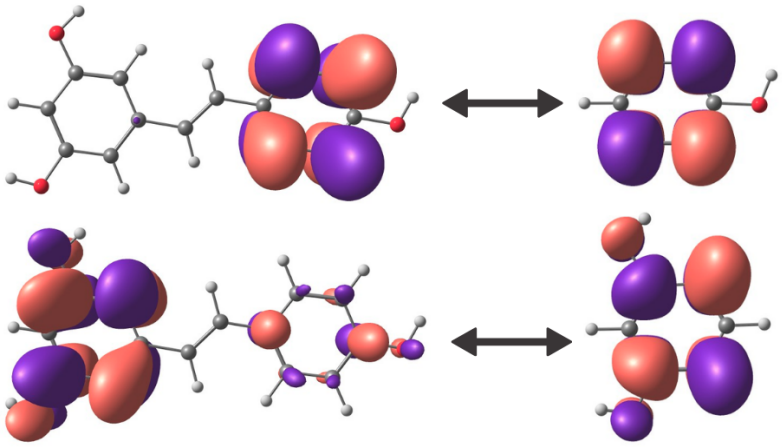

Figure 4.12: Similarity between π_2^* and π_3^* RV orbitals with PH and RS orbitals, respectively.

Chapter 5

Transient Anion States of Resveratrol and Resorcinol

This chapter is dedicated to discuss the anion states of RS and RV. We estimate its energies from the cross sections for elastic electron scattering for the (a)-RS, (c)-RS and p-RV geometries. Subsequently, we infer possible dissociation fragments initiated by the anion states from the analysis of virtual orbitals and reaction thresholds for the (a)-RS, (c)-RS and PH compounds.

The target electronic ground state was described at the restricted Hartree-Fock level, with a set of Cartesian Gaussian basis set generated as described by *Bettega et al.* [48, 49]. We employed 5s5p2d basis sets for the carbon and oxygen atoms and the 4s basis set reported by *Dunning* [50] for the hydrogen atoms, as reported in Tabs. 5.1 and 5.2, resulting in a total of 274 basis functions for each RS geometry and 580 for RV. The elastic scattering cross sections were computed with the parallel version [68] of the SMCPP method in the SE and SEP approximations. Sets of MVOs were generated from the cationic Fock operators with charge +6 for RS and +8 for RV. The configuration space was built by including all CSFs that satisfy $\epsilon_{scatt} + \epsilon_{part} - \epsilon_{hole} < \Delta$, where ϵ_{scat}, ϵ_{part}, and ϵ_{hole} are the energies of the scattering, particle, and hole orbitals, respectively, while Δ is a cutoff. For RS the symmetries of both geometries were explored, and we used $\Delta = -0.85$ hartee resulting in 10053 configurations for the A_1 component of the CSF space, and $\Delta = -1$ hartee for A_2, B_1 and B_2 generating 6633, 6724 and 6654 configurations, respectively. Similarly,

Table 5.1: Gaussian-Cartesian sets employed in the scattering and target calculations. The exponents for the carbon and oxygen atoms are given in atomic units.

Type	Carbon	Oxygen
s	12.49408	16.05878
s	2.47029	5.92024
s	0.61402	1.03490
s	0.18402	0.31684
s	0.03998	0.06520
p	5.22886	10.14120
p	1.59205	2.78299
p	0.56861	0.84100
p	0.21032	0.23293
p	0.07225	0.07764
d	0.60359	0.75679
d	0.15675	0.18075

Table 5.2: Gaussian-Cartesian employed sets employed in the scattering and target calculations. The exponents for the hydrogen atom are given in atomic units.

Type	Exponent	Coefficient
s	13.3615	0.130844
s	2.0133	0.921539
s	0.4538	1.000000
s	0.1233	1.000000

we used $\Delta = 0.95$ hartee for A' and A'' components generating 15405 and 15228 configurations, respectively. For p-RV, only the A'' component of CSF space were obtained, since we do not expect resonance signatures if the A' cross section, we employed a higher cutoff ($\Delta = -1.3$ hartree) to reduce the computational effort, which results in 17969 CFSs. Finally, the reaction thresholds for H and H_2 were estimated with the composite G4(MP2) method [69].

5.1 Scattering Results

The integral cross sections (ICSs) obtained for (c)-RS in the SE and SEP approximations are shown in Fig. 5.1, while Fig. 5.2 presents a comparison between (a)-RV and (c)-RV ICS in the SEP approximation. The resonances positions and auto-ionization widths were estimated with Eq. 3.46 using a third order polynomial as the background. In the SE calculations, we obtained three π^* shape resonances for

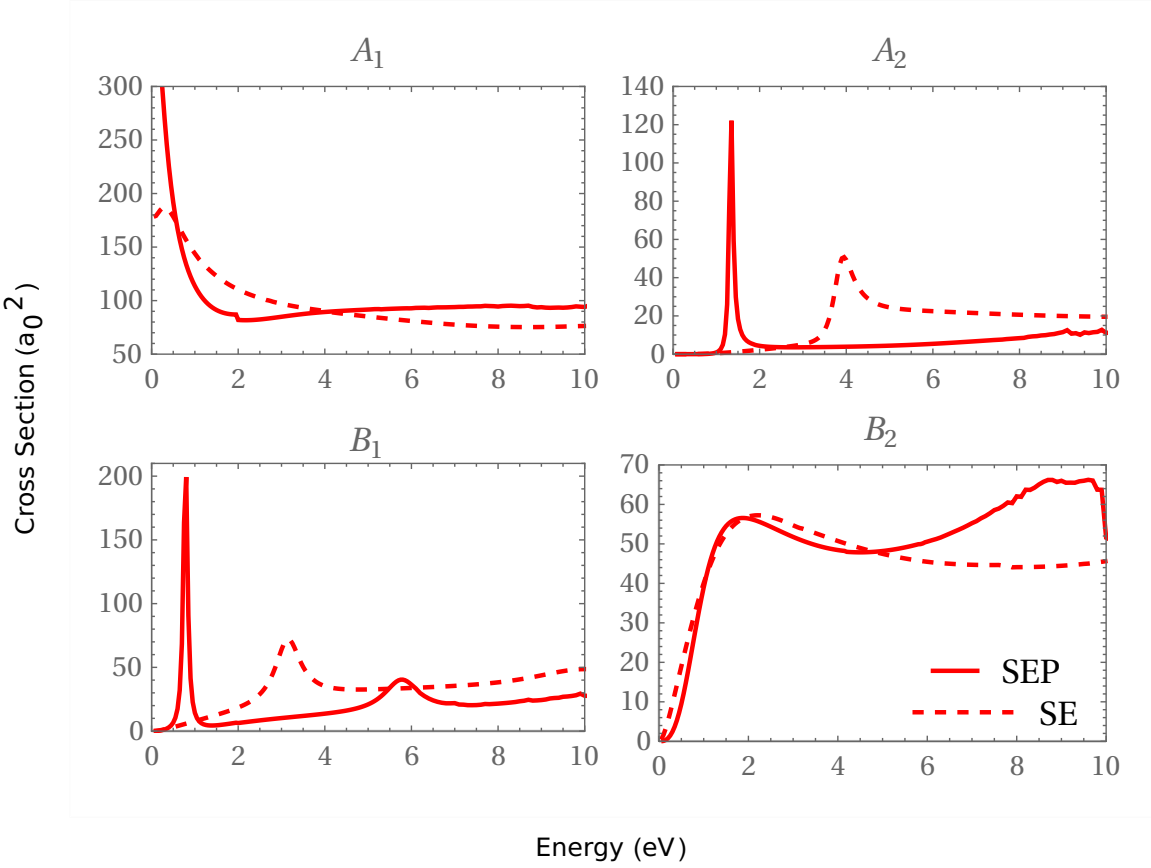

Figure 5.1: Symmetry decomposition of the integral cross section for elastic electron scattering by RS. The calculations were performed for the the structure (c) in the SE (dotted line) and SEP (solid line).

both geometries, two of them in the B_1 symmetry, located at 3.15 eV and 9.95 eV, and the other one in A_2, located at 3.92 eV for (c)-RS. The three resonances are found in the A'' symmetry for (a)-RS, around 3.10 eV, 3.88 eV and 9.89 eV. When polarization effects are taken into account, these anions states are shifted to lower energies, specifically, 0.78 eV and 5.78 eV (B_1 symmetry), and 1.34 eV (A_2 symmetry) for (c)-RS, while 0.75 eV, 1.21 eV and 5.70 eV for (a)-RS. The resonance positions obtained for the two structures are in good agreement. The results for the π_1^* and π_2^* resonances are consistent with those obtained from the empirical rescaling of virtual orbitals energies (see Tab. 4.3), although a larger discrepancy is found for the π_3^* state. This kind of disagreement is typical of π^* resonances having mixed shape and core-excited character and is related to the neglect of electronic excitation channels in the scattering calculations [70, 71]. Despite the fact that the excited states are described by single excitations in our calculations, the threshold for the first triplet

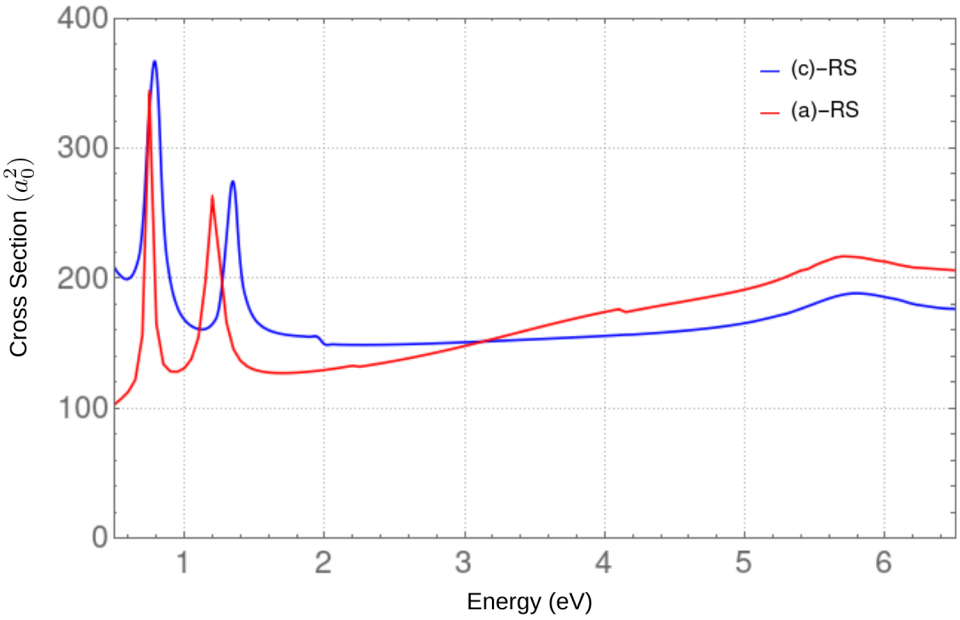

Figure 5.2: Integral cross section for elastic electron scattering by the (a) (red line) and (c) (blue line) structures of RS.

estimated with the CASPT2 method (3.9 eV, see Chap. 4) indeed suggest the possibility of a mixed-character resonance. The oscillations in the A_2 and B_2 components of the cross sections (Fig. 5.1) are spurious resonances that also arise from the elastic scattering approximation in the SEP calculations, i.e., for treating energetically open channels as closed.

The SMCPP method allows the diagonalization of the scattering Hamiltonian represented in the square integrable CSF basis. The eigenstates are said to be pseudo-states since they do not have the asymptotic boundary condition, but they are useful to interpret the calculated resonance spectra. The orbital plots shown in Fig. 5.3 were obtained from the SE-approximation pseudo-eigenstates, in which the scattering orbitals can be expressed as linear combinations of MVOs, according to Eq. 3.44. We only show the orbitals for the (c)-RS structure but we perform a similar analysis for the (a)-RS structure, obtaining similar results. It is interesting to note that the orbitals in Fig. 5.3 are compatible to the virtual orbitals computed with compact basis sets (Fig. 4.4), which are often useful to assign resonance characters, the only relevant difference being the amplitudes around the oxygen atoms for the π_3^* state.

Tab. 5.3 summarizes the positions and widths of the π^* anion states of the RS

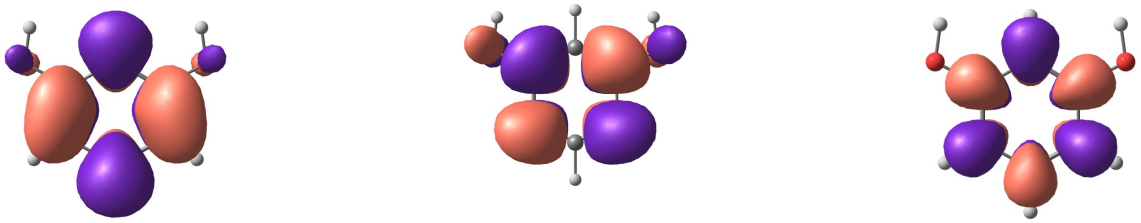

(a) π_1^* (b) π_2^* (c) π_3^*

Figure 5.3: π^* type orbitals obtained from the pseudo-eigenstates of the scattering Hamiltonian. The orbitals are linear combinations of the MVOs employed in the scattering calculation and provide insight into the characters of the resonances.

molecule obtained for both geometries. The widths are also compatible for both geometries, with the exception of π_1^* at SEP approximation. However, the difference is rather small in absolute value (50 meV), bearing in mind the numerical procedures.

Table 5.3: Resonance energy (in eV) and ionization widths (in eV), given in parenthesis parentheses, for the (a)- and (c)-RS geometries calculated in SE and SEP approximations.

	(c)-RS		(a)-RS	
	SE	SEP	SE	SEP
π_1^*	3.15 (0.72)	0.78 (0.11)	3.10 (0.65)	0.75 (0.05)
π_2^*	3.92 (0.59)	1.34 (0.11)	3.88 (0.61)	1.21 (0.12)
π_3^*	9.95 (2.91)	5.78 (1.02)	9.89 (2.62)	5.70 (0.91)

In Fig. 5.4 we show the A'' component of the ICS for p-RV. In the SE calculations, we obtained five π^* shape resonances, located at 0.72 eV (π_1^*), 2.09 eV (π_2^*), 4.02 eV (π_3^*), 6.10 eV (π_4^*) and 10.24 eV (π_5^*). The interpretation of the SEP results for this system turned out to be more challenging, since we observed only three π^* shape resonances, located at 0.44 eV, 2.05 eV and 3.81 eV. The π_1^* resonance became an anionic bound state with the vertical energy of -0.07 eV, as expected (see Tab. 4.7). Its binding energy was obtained from the diagonalization of the scattering Hamiltonian in the CSF basis, as show in Fig 5.5. There seems to be on missing resonance in the ICS because the π_3^* and π_4^* lie very close to each other in our calculations, and their signatures merge into a single peak. Finally the signature of the π_5^* state, expected to have mixed character, is found at 3.8 eV.

The resonance spectra obtained from the ICS and from the empirical scaling relation are compared in Tab. 5.4. When more than a single resonance is found in

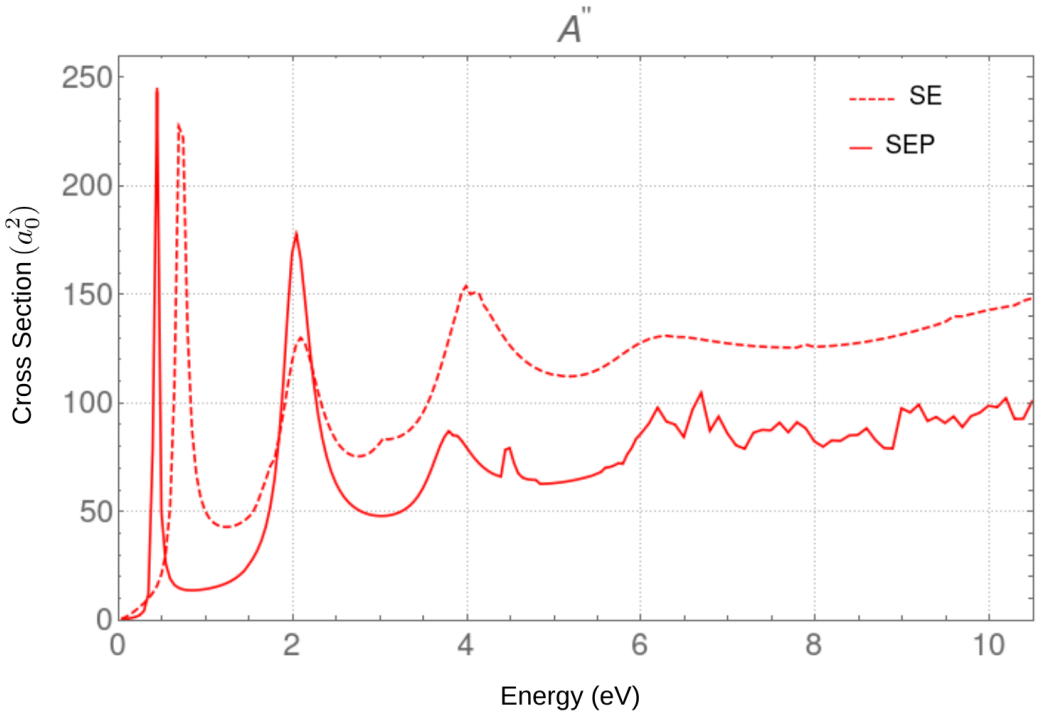

Figure 5.4: A'' integral cross section of neutral p-RV calculated in SE - dashed line - and SEP - filled line - approximations.

the same symmetry component, it is not a simple task to obtain a balanced description (among the anion states) of the correlation-polarization effects [53], so RV is a very challenging system in this respect. In addition, there is no molecule as large as RV in the data set used to establish the scaling relation (nor molecules with more than one unsaturated ring) [58], so it is not clear how reliable the scaling would be for RV.

There is a reasonable agreement between both calculations for the four lowest-lying π^* resonances, in particular the prediction of a shallow bound state and two nearly-degenerate resonances, in spite of the 0.4 eV discrepancies for the positions of the π_2^* and (π_3^*, π_4^*) anion states. The more significant disagreement for the π_5^* state is not surprising in view of the expected mixed character, as discussed above, while the π_6^* and π_7^* states, in case they exist at all, lie well into the electronic excitation region.

The pseudo-eigenstates of the scattering Hamiltonian were found particularly useful to assign the RV resonances. The weights of the MVOs in the expansion of the scattering orbitals accounting for electron attachment are shown in Fig. 5.5, and the amplitudes of the corresponding pseudo-eigenstates are shown in Fig. 5.6.

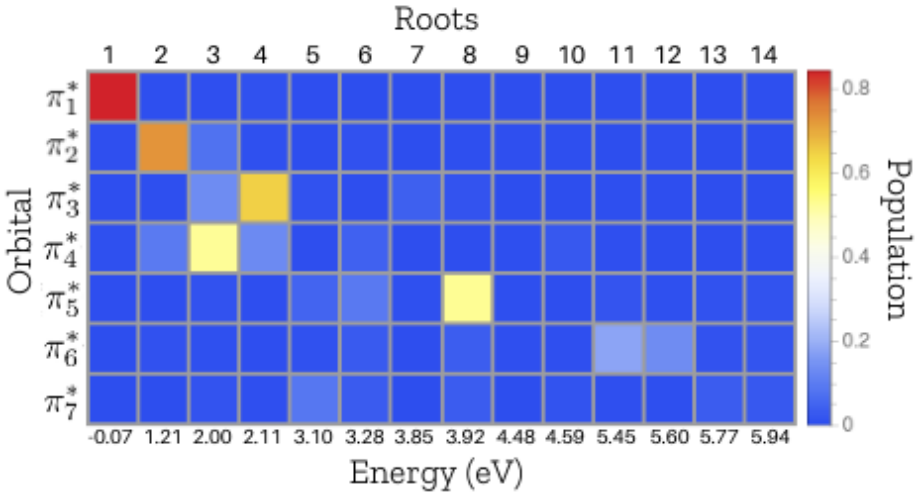

Figure 5.5: Low-lying pseudo-eigenstates of the scattering Hamiltonian represented in the SEP-approximation CSF space for p-RV. The horizontal axis corresponds to the pseudo-eigenvalues, the vertical axis to the MVOs with π^* character and the color map indicates the weights of these MVOs in the pseudo-eigenstates that can be viewed as approximations to the resonance states of present interest.

Table 5.4: Resonance positions (in eV) and ionization widths (in eV), given in parenthesis, for the p-RV geometry calculated with SE and SEP approximations. The negative position indicates a bound anion state and the VAE estimates were obtained from the empirical scaling relation (see Chap. 4)

Orbitals	SE	SEP	VAE
π_1^*	0.72(0.13)	-0.07	-0.05
π_2^*	2.09(0.54)	0.44(0.05)	0.85
π_3^*	4.02(0.91)	2.05(0.39)	1.46
π_4^*	6.10(2.12)	2.05(0.39)	1.56
π_5^*	10.24(2.46)	3.81(0.56)	2.82
π_6^*	-	-	4.76
π_7^*	-	-	5.15

In principle we could try to augment the CSF space in the SMC simulations, but the additional computational cost would be significant. Our results seem to be reasonable and the accuracy of the method when compared to electron transmission data is typically around 0.3 eV, such that the cost-benefit of a more expensive calculation could be questioned.

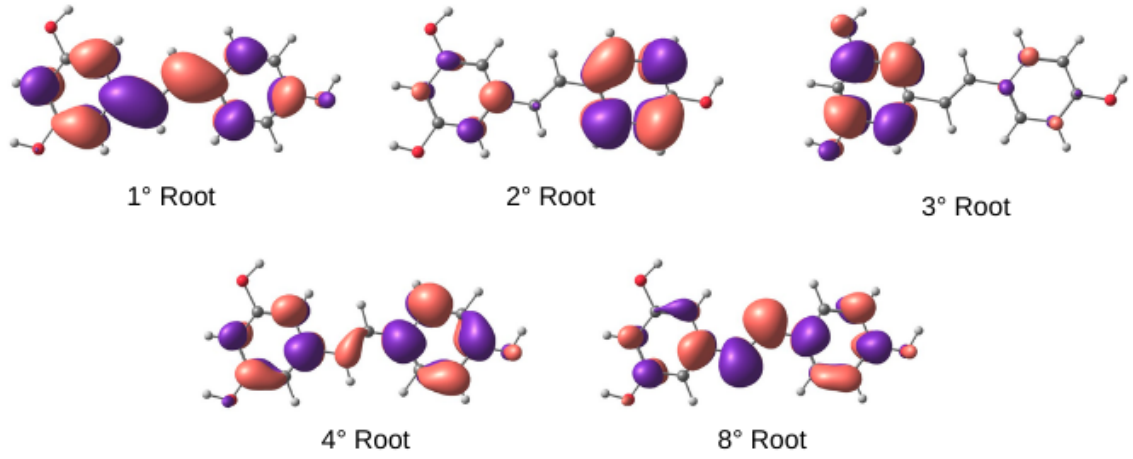

Figure 5.6: Pseudo-eigenstates of the scattering Hamiltonian for p-RV. The orbital amplitudes correspond to the pseudo states shown in Fig. 5.5.

5.2 Discussion

We can also analyze the RV anionic states by decomposing the molecule into the subunits: RS and PH. The PH shape resonance spectrum is known theoretically and experimentally [72–74]. The molecule has three π^* shape resonances, represented by the compact virtual orbitals shown in Fig. 5.7. The two resonance of RV which are localized on a single subunit have a clear correspondence with the resonances of the subunits, i.e., the π_2^* and π_3^* states of RV correlate with the π_1^* state in PH and the π_2^* state in RS, respectively. Tab. 5.5 shows experimental and theoretical results obtained for these two resonances. There is a reasonable correspondence between subunits SEP calculations and RV scaling relation. The resonances could be expected to stabilize in RV with respect to the monomers since there is some degree of delocalization, and mutual polarization of the subunits. This was not the case for the π_3^* resonance in RV, corresponding to π_2^* in RS, although we did not further investigate this point.

Table 5.5: Resonance positions (in eV) of PH, RS and RV molecules calculated with the SEP approximation [72, 73]. Exp. and SR states for Experimental and Scaling Relation results. For more information see the text.

PH		(a)-RS	p-RV	
SEP	Exp.	SEP	SEP	SR
0.91 (π_1^*)	1.01 (π_1^*)	0.75 (π_1^*)	0.44 (π_2^*)	0.85 (π_2^*)
1.33 (π_2^*)	1.73 (π_2^*)	1.21 (π_2^*)	2.05 (π_3^*)	1.46 (π_3^*)

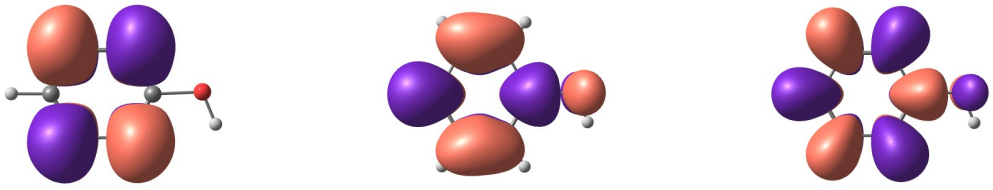

(a) π_1^* (b) π_2^* (c) π_3^*

Figure 5.7: Compact virtual orbitals of the PH molecule representing π^* shape resonances. The orbitals were generated with the ωB97XD/6-31G* method.

Table 5.6: Anion fragments observed in DEA experiment [7]. The fragments, the energy positions of the peaks (in eV) and the relative intensities are shown.

Fragment	Energy	Intensity
M^-	0.0	45
$[M\text{-}H]^-$	1.2	100
	4.3	24
$[M\text{-}2H]^-$	0.0	17
	0.6	*
$[M\text{-}3H]^-$	4.5	0.8
	9.5	1.3
$[M\text{-}(CH)_2OH]^-$	8.7	0.8

DEA to RV was investigated experimentally [7]. In this experiment, the mass of anionic fragments are observed as a function of the incident energy of the electrons. It is worth mentioning that the RV molecule was evaporated at 170° C and the collision cell was kept at 180° C to avoid condensation. Even for this high temperature, a relevant population of the c-RV isomer is not expected. A more detailed description of the experimental procedure can be found at Ref. [10]. The main fragments reported by in Ref. [7] are reproduced in Tab. 5.6, along with the energies of the signal peaks and their relative intensities. We employ the notation $[M\text{-}X]^-$ to denote the anion fragment formed by the release of the neutral fragment X from the parent M-molecular anion. For instance, the hydrogen elimination reaction corresponds to

$$M + e^- \rightarrow [M - H]^- + H\,.$$

Unfortunately, we could not calculate dissociation thresholds for the RV molecule with the G4(MP2) method due to hardware limitations, although zero-energy thresholds obtained form DFT computations were reported in Ref. [7]. In the following,

we restrict the discussion to the lower-energy fragments since our calculations do not account for core-excited resonances.

The calculated energy of the π_2^* state, 0.44 eV (or 0.85 eV according to the empirical estimate), is compatible with the DEA peak for the elimination of two hydrogens (0.6 eV). The nearly degenerate resonances, π_3^* and π_4^*, are expected to give rise to the most intense DEA signal (1.2 eV), corresponding the the H-elimination reaction. This is an indication that our scattering calculations overestimate the resonance positions (2.0 eV), and in fact the empirical estimate is more reasonable (1.5 eV). Finally, the DEA peaks around 4 eV are compatible with the π_5^* resonance, which is predicted at 3.8 eV (SMCPP) or 2.8 eV (empirical estimate). In this case the SMCPP result is in better agreement with the data, but both predictions can be questioned because core-excited anion states could play a role around 4.0 eV. Turning attention to the DEA signals at 0 eV, one should remind the shallow valence bound anion state (π_1^*). While we could not converge a DBS calculation, due to numerical difficulties, the dipole moment of the RV molecule can exceed 3.0 D in case the hydroxyl groups in the RS subunit are properly aligned, so a shallow DBS could also be expected. As a result, two bound anion states could give rise to vibrational Feshbach resonances which are consistent with the DEA data at 0 eV. The observation of the parent anion (M^-) suggests stabilization by vibrational energy redistribution, while the elimination of two hydrogen atoms should be favored by the formation of H_2, a very stable reaction product.

The abstraction of one or more H atoms in DEA reactions should involve σ^* resonances with anti-bonding character in the polar OH groups. This resonances typically do not have clear signatures in the scattering cross sections [6, 75]. It is a common practice in the research group to look for indirect evidence of those σ^* states in the virtual orbitals calculated with compact basis sets. As shown in Fig. 5.8, not only we could find anti-bonding virtual orbitals with σ_{OH}^* character, but they also have similar amplitudes as those calculated for the PH and RS subunits.

As previously observed, the DEA reaction that produces H_2 has been claimed

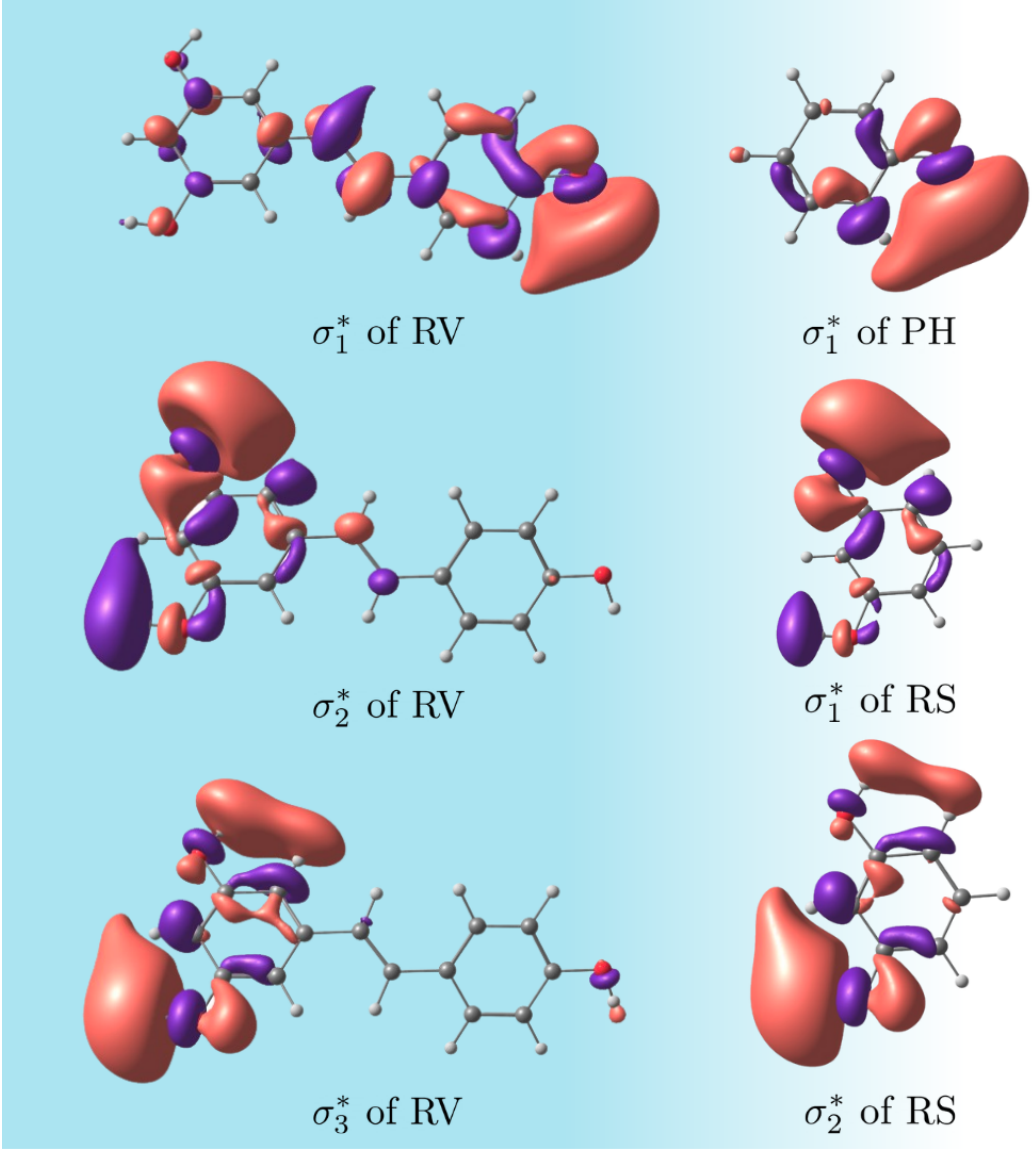

Figure 5.8: σ^* virtual orbitals obtained with the ωB97XD/6-31G* for the RV (most stable geometry), RS and PH molecules.

relevant for the antioxidant activity of RV [7]. The RV molecule, especially in view of its size, is a very challenging system for scattering and even bound-state simulations, so we proposed RS as a prototype in the present study, since H_2 is likely to be produced in the RS subunit of RV, where two hydroxyl groups lie close to each other.

The calculated reaction thresholds for the H-elimination channels are shown in Tab. 5.7 for both RS conformers (the atomic labels are given in Fig. 5.9). The formation of H_2, along with the meta-benzoquinone (MBQ) anion, has a nearly zero threshold at 0 K, and the reaction becomes exothermic at higher temperatures. While in this respect RS would be similar to RV, since the latter produces H_2 at 0 eV, the

absence of anion bound states in RS should suppress DEA at 0 eV, since the reactions are expected to be initiated by vibrational Feshbach resonances. The dissociation thresholds for both RS structures are typically above the energy of the π_1^* resonance (0.8 eV, see Tab. 5.7). Therefore, H elimination would not proceed from the formation of the π_1^* state, although H_2 elimination is energetically allowed. Based only on the energetics, one could expect elimination of H and H_2 initiated by the π_2^* resonance (1.4 eV). Of course DEA processes should also be initiated by higher-lying anion states, but we do not discuss those processes here.

For completeness, we also show the dissociation thresholds for the PH subunit in Tab. 5.7. While we do not discuss the details here, since this molecules was studied previously, in general our estimates are consistent with the DEA data [72–74]. The thresholds are slightly higher for PH than RS, and it is also clear that this subunit cannot produce H_2 at lower energies (H abstraction for CH bonds is energetically less favorable than from the polar OH bonds). These results provide further evidence that the PH subunit can contribute to the DEA channels releasing H atoms from RV, but it should not be involved in the production of molecular hydrogen.

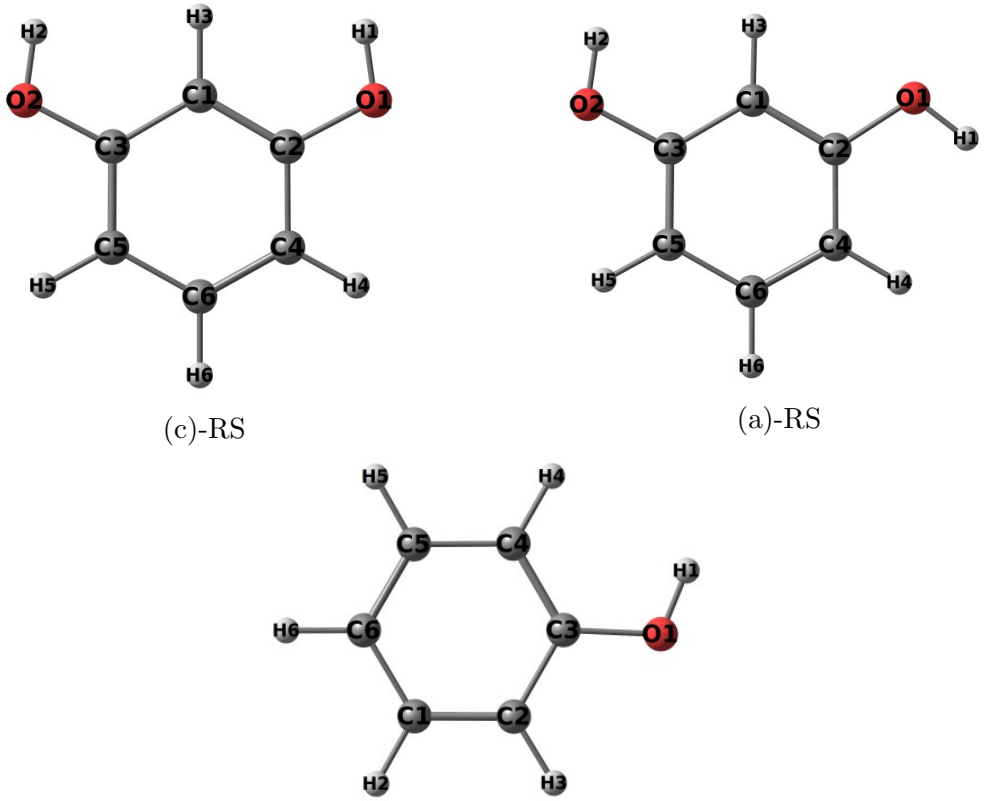

Figure 5.9: Atomic labels for the (a)-RS (top right), (c)-RS (top left) and PH (bottom) molecules used as references for the dissociation thresholds given in Tab. 5.7.

Table 5.7: Dissociation thresholds (in eV) at zero temperature (ΔE) and finite temperatures, corresponding to free energies (ΔG) at 298.15 K and 453.15 K. The calculations were performed with the G4(MP2) method and the atomic labels are given in Fig. 5.9.

Reaction	ΔE	$\Delta G_{(298.15)}$	$\Delta G_{(453.15)}$
(c)-RS+e^- → MBQ$^{\bullet-}$+H_2	-0.01	-0.33	-0.55
(c)-RS+e^- → [(c)-RS - H1]$^-$+H$^\bullet$	1.30	0.99	0.80
(c)-RS+e^- → [(c)-RS - H2]$^-$+H$^\bullet$	1.30	0.99	0.80
(c)-RS+e^- → [(c)-RS - H3]$^-$+H$^\bullet$	2.51	2.23	1.96
(c)-RS+e^- → [(c)-RS - H4]$^-$+H$^\bullet$	3.42	3.10	2.90
(c)-RS+e^- → [(c)-RS - H6]$^-$+H$^\bullet$	3.55	3.27	3.00
(a)-RS+e^- → MBQ$^{\bullet-}$+H_2	0.02	-0.28	-0.49
(a)-RS+e^- → [(a)-RS - H2]$^-$+H$^\bullet$	1.33	1.04	0.86
(a)-RS+e^- → [(a)-RS - H1]$^-$+H$^\bullet$	1.37	1.08	0.89
(a)-RS+e^- → [(a)-RS - H3]$^-$+H$^\bullet$	2.87	2.48	2.36
(a)-RS+e^- → [(a)-RS - H5]$^-$+H$^\bullet$	3.03	2.74	2.55
(a)-RS+e^- → [(a)-RS - H4]$^-$+H$^\bullet$	3.43	3.13	2.94
(a)-RS+e^- → [(a)-RS - H6]$^-$+H$^\bullet$	3.43	3.14	2.94
PH + e^- → [PH - H1]$^-$+H$^\bullet$	1.42	1.14	0.95
PH + e^- → [PH - H4]$^-$+H$^\bullet$	3.03	2.75	2.56
PH + e^- → [PH - H3]$^-$+H$^\bullet$	3.43	3.14	2.94
PH + e^- → [PH - H5]$^-$+H$^\bullet$	3.48	3.19	3.00
PH + e^- → [PH - H2]$^-$+H$^\bullet$	3.55	3.26	3.07
PH + e^- → [PH - H6]$^-$+H$^\bullet$	3.60	3.31	3.11

Chapter 6

Conclusion

We reported the first theoretical investigation on the low-energy anion spectra of the polyphenolic compounds RV and RS. RV is a very challenging system for this kind of study in view of its size. While the polarization effects do not seem properly balanced between in the anion states in the SEP calculations, our results point out a valence bound state, three shape resonances and a mixed-character resonance. Resonances could trigger H abstraction in the RV molecule, but the dissociation threshold energy could not be estimated with the G4(MP2) method. The zero-energy thresholds reported elsewhere and the presently calculated resonance spectrum are consistent with the DEA data. In particular, with the production of H_2 at nearly zero energy which could proceed from vibrational Feshbach resonances arising from the valence bound state. We suspect a DBS could also play a role, but we could not converge the calculation so far.

We also investigated the RS subunit, which could be a less computationally expensive prototype for the production of H_2, a reaction that could account for the antioxidant activity of RV. We obtained two π^* shape resonances and a mixed-character resonance with the SEP calculations. There is a correspondence between the anion states of RV and RS, and even between the thresholds, but the lack of anion bound states for the smaller molecules should suppress the H_2-formation channel at 0 eV.

The inclusion of solvation effects in the anionic states is in perspective for future studies. Our group is developing methods to describe the transient anion states in solution. We could expect the π_1^* state to become more stable in water environment,

such that RS could be a better prototype for H_2 production in this case. The DBS, on the other hand, should be less important in a polarizable dielectric environment such as water.

Bibliography

[1] Ilya I Fabrikant, Samuel Eden, Nigel J Mason, and Juraj Fedor. Recent progress in dissociative electron attachment: from diatomics to biomolecules. In *Advances in atomic, molecular, and optical physics*, volume 66, pages 545–657. Elsevier, 2017. [Cited on pages 1 and 2.]

[2] Eliane M de Oliveira, Sergio d'A Sanchez, Márcio HF Bettega, Alexandra PP Natalense, Marco AP Lima, and Márcio T do N Varella. Shape resonance spectra of lignin subunits. *Physical Review A*, 86(2):020701, 2012. [Cited on page 8.]

[3] Badia Boudaıffa, Pierre Cloutier, Darel Hunting, Michael A Huels, and Léon Sanche. Resonant formation of dna strand breaks by low-energy (3 to 20 ev) electrons. *Science*, 287(5458):1658–1660, 2000. [Cited on page 1.]

[4] Carl Winstead and Vincent McKoy. Electron–molecule collisions in low-temperature plasmas: the role of theory. 2000. [Cited on page 1.]

[5] Winifred M Huo and Y-K Kim. Electron collision cross-section data for plasma modeling. *IEEE Transactions on plasma Science*, 27(5):1225–1240, 1999. [Cited on page 1.]

[6] LM Cornetta, F Kossoski, and MT do N Varella. Transient anion spectra of the potential radiosensitizers 5-cyanateuracil and 5-thiocyanateuracil. *The Journal of Chemical Physics*, 147(21):214310, 2017. [Cited on pages 1 and 74.]

[7] Stanislav A Pshenichnyuk and Alexei S Komolov. Dissociative electron attachment to resveratrol as a likely pathway for generation of the h_2 antioxidant species inside mitochondria. *The journal of physical chemistry letters*, 6(7):1104–1110, 2015. [Cited on pages xiii, xviii, 1, 6, 7, 57, 73, and 75.]

[8] Joseph A Baur and David A Sinclair. Therapeutic potential of resveratrol: the in vivo evidence. *Nature reviews Drug discovery*, 5(6):493, 2006. [Cited on pages 1 and 6.]

[9] Charles Jean Joachain. *Quantum collision theory*. 1975. [Cited on pages 2, 39, and 40.]

[10] Stanislav A Pshenichnyuk, Alberto Modelli, and Alexei S Komolov. Interconnections between dissociative electron attachment and electron-driven biological processes. *International Reviews in Physical Chemistry*, 37(1):125–170, 2018. [Cited on pages xiii, 2, 4, 5, and 73.]

[11] Lucas Medeiros Cornetta. *Processos eletro-induzidos em complexos de timina e uracila.* PhD thesis, Universidade de São Paulo, 2019. [Cited on pages xiii and 3.]

[12] F Kossoski, MT do N Varella, and M Barbatti. On-the-fly dynamics simulations of transient anions. *The Journal of Chemical Physics*, 151(22):224104, 2019. [Cited on pages 3 and 4.]

[13] David E Metzler. *Biochemistry (2 Volume Set): The Chemical Reactions of Living Cells.* Elsevier, 2003. [Cited on page 4.]

[14] AB Rubin, Vladimir Pavlovich Shinkarev, and AA Kononenko. Electron transport in biological systems. 1984. [Cited on page 4.]

[15] Lindsey N Pelster and Shelley D Minteer. Mitochondrial inner membrane biomimic for the investigation of electron transport chain supercomplex bioelectrocatalysis. *ACS Catalysis*, 6(8):4995–4999, 2016. [Cited on page 4.]

[16] Michael P Murphy. How mitochondria produce reactive oxygen species. *Biochemical journal*, 417(1):1–13, 2008. [Cited on page 4.]

[17] Werner JH Koopman, Peter HGM Willems, and Jan AM Smeitink. Monogenic mitochondrial disorders. *New England Journal of Medicine*, 366(12):1132–1141, 2012. [Cited on page 4.]

[18] A Yu Andreyev, Yu E Kushnareva, and AA Starkov. Mitochondrial metabolism of reactive oxygen species. *Biochemistry (Moscow)*, 70(2):200–214, 2005. [Cited on page 4.]

[19] RAP Costa, Carolina Domeniche Romagna, JL Pereira, and Nadja Cristhina Souza-Pinto. The role of mitochondrial dna damage in the citotoxicity of reactive oxygen species. *Journal of bioenergetics and biomembranes*, 43(1):25–29, 2011. [Cited on page 4.]

[20] Julio F Turrens. Mitochondrial formation of reactive oxygen species. *The Journal of physiology*, 552(2):335–344, 2003. [Cited on page 5.]

[21] Qun Chen, Edwin J Vazquez, Shadi Moghaddas, Charles L Hoppel, and Edward J Lesnefsky. Production of reactive oxygen species by mitochondria central role of complex iii. *Journal of Biological Chemistry*, 278(38):36027–36031, 2003. [Cited on page 5.]

[22] Adam Szewczyk and Lech Wojtczak. Mitochondria as a pharmacological target. *Pharmacological reviews*, 54(1):101–127, 2002. [Cited on page 5.]

[23] John E Biaglow. Cellular electron transfer and radical mechanisms for drug metabolism. *Radiation research*, 86(2):212–242, 1981. [Cited on page 5.]

[24] James S Wright, Erin R Johnson, and Gino A DiLabio. Predicting the activity of phenolic antioxidants: theoretical method, analysis of substituent effects, and application to major families of antioxidants. *Journal of the American Chemical Society*, 123(6):1173–1183, 2001. [Cited on page 6.]

[25] Alberto Modelli and Stanislav A Pshenichnyuk. Gas-phase dissociative electron attachment to flavonoids and possible similarities to their metabolic pathways. *Physical Chemistry Chemical Physics*, 15(5):1588–1600, 2013. [Cited on page 6.]

[26] Ikuroh Ohsawa, Masahiro Ishikawa, Kumiko Takahashi, Megumi Watanabe, Kiyomi Nishimaki, Kumi Yamagata, Ken-ichiro Katsura, Yasuo Katayama, Sadamitsu Asoh, and Shigeo Ohta. Hydrogen acts as a therapeutic antioxidant by selectively reducing cytotoxic oxygen radicals. *Nature medicine*, 13(6):688, 2007. [Cited on page 6.]

[27] Stanislav A Pshenichnyuk and Alexei S Komolov. Dissociative electron attachment to anthralin to model its biochemical reactions. *The journal of physical chemistry letters*, 5(16):2916–2921, 2014. [Cited on page 7.]

[28] Raj B Durairaj. *Resorcinol: chemistry, technology and applications*. Springer Science & Business Media, 2005. [Cited on page 8.]

[29] Jamie D Young, Michael Staniforth, Adam S Chatterley, Martin J Paterson, Gareth M Roberts, and Vasilios G Stavros. Relaxation dynamics of photoexcited resorcinol: internal conversion versus h atom tunnelling. *Physical Chemistry Chemical Physics*, 16(2):550–562, 2014. [Cited on page 8.]

[30] F. Jensen. *Introduction to Computational Chemistry*. Wiley, 2017. [Cited on pages 9, 20, 21, 22, 24, and 35.]

[31] Linus Pauling and E Bright Wilson. *Introduction to quantum mechanics with applications to chemistry*. Courier Corporation, 2012. [Cited on pages 22 and 33.]

[32] KI Ramachandran, Gopakumar Deepa, and Krishnan Namboori. *Computational chemistry and molecular modeling: principles and applications*. Springer Science & Business Media, 2008. [Cited on page 9.]

[33] Gerhard Herzberg and Bryce L Crawford Jr. Infrared and raman spectra of polyatomic molecules. *The Journal of Physical Chemistry*, 50(3):288–288, 1946. [Cited on page 10.]

[34] Max Born and Kun Huang. *Dynamical theory of crystal lattices*. Clarendon press, 1954. [Cited on page 11.]

[35] Richard Phillips Feynman. Forces in molecules. *Physical review*, 56(4):340, 1939. [Cited on page 13.]

[36] Robert O Jones. Density functional theory: Its origins, rise to prominence, and future. *Reviews of modern physics*, 87(3):897, 2015. [Cited on page 25.]

[37] Carlos Fiolhais, Fernando Nogueira, and Miguel AL Marques. *A primer in density functional theory*, volume 620. Springer Science & Business Media, 2003. [Cited on page 25.]

[38] E. Engel and R.M. Dreizler. *Density Functional Theory: An Advanced Course*. Theoretical and Mathematical Physics. Springer Berlin Heidelberg, 2011. [Cited on pages 25 and 34.]

[39] John P Perdew and Alex Zunger. Self-interaction correction to density-functional approximations for many-electron systems. *Physical Review B*, 23(10):5048, 1981. [Cited on page 34.]

[40] Axel D Becke. A new mixing of hartree–fock and local density-functional theories. *The Journal of chemical physics*, 98(2):1372–1377, 1993. [Cited on page 35.]

[41] Jiří Klimeš and Angelos Michaelides. Perspective: Advances and challenges in treating van der waals dispersion forces in density functional theory. *The Journal of chemical physics*, 137(12):120901, 2012. [Cited on page 35.]

[42] Jeng-Da Chai and Martin Head-Gordon. Long-range corrected hybrid density functionals with damped atom–atom dispersion corrections. *Physical Chemistry Chemical Physics*, 10(44):6615–6620, 2008. [Cited on page 35.]

[43] Claudio Morgado, Mark A Vincent, Ian H Hillier, and Xiao Shan. Can the dft-d method describe the full range of noncovalent interactions found in large biomolecules? *Physical Chemistry Chemical Physics*, 9(4):448–451, 2007. [Cited on page 35.]

[44] Jeng-Da Chai and Martin Head-Gordon. Systematic optimization of long-range corrected hybrid density functionals. *The Journal of chemical physics*, 128(8):084106, 2008. [Cited on page 35.]

[45] Stefan Grimme. Semiempirical gga-type density functional constructed with a long-range dispersion correction. *Journal of computational chemistry*, 27(15):1787–1799, 2006. [Cited on page 36.]

[46] Marco AP Lima and Vincent McKoy. Aspects of the schwinger multichannel variational formulation. *Physical Review A*, 38(1):501, 1988. [Cited on pages 41, 42, and 43.]

[47] Romarly F da Costa, Márcio T do N Varella, Márcio HF Bettega, and Marco AP Lima. Recent advances in the application of the schwinger multichannel method with pseudopotentials to electron-molecule collisions. *The European Physical Journal D*, 69(6):159, 2015. [Cited on pages 41, 42, and 43.]

[48] MHF Bettega, LG Ferreira, and MAP Lima. Transferability of local-density norm-conserving pseudopotentials to electron-molecule-collision calculations. *Physical Review A*, 47(2):1111, 1993. [Cited on pages 44, 45, and 65.]

[49] GB Bachelet, DR Hamann, and M Schlüter. Pseudopotentials that work: From h to pu. *Physical Review B*, 26(8):4199, 1982. [Cited on pages 44, 45, and 65.]

[50] Thom H Dunning Jr. Gaussian basis functions for use in molecular calculations. i. contraction of (9s5p) atomic basis sets for the first-row atoms. *The Journal of Chemical Physics*, 53(7):2823–2833, 1970. [Cited on pages 45 and 65.]

[51] Marco AP Lima, Luiz M Brescansin, Antonio JR da Silva, Carl Winstead, and Vincent McKoy. Applications of the schwinger multichannel method to electron-molecule collisions. *Physical Review A*, 41(1):327, 1990. [Cited on page 45.]

[52] Antônio JR da Silva, Marco AP Lima, Luiz M Brescansin, and Vincent McKoy. Schwinger multichannel method: A study of a feshbach resonance in e-h 2 collisions. *Physical Review A*, 41(5):2903, 1990. [Cited on page 46.]

[53] F Kossoski and MHF Bettega. Low-energy electron scattering from the aza-derivatives of pyrrole, furan, and thiophene. *The Journal of Chemical Physics*, 138(23):234311, 2013. [Cited on pages 47 and 70.]

[54] Charles W Bauschlicher Jr. The construction of modified virtual orbitals (mvo's) which are suited for configuration interaction calculations. *The Journal of Chemical Physics*, 72(2):880–885, 1980. [Cited on page 47.]

[55] Charles Desfrançois, Hassan Abdoul-Carime, and Jean-Pierre Schermann. Ground-state dipole-bound anions. *International Journal of Modern Physics B*, 10(12):1339–1395, 1996. [Cited on page 49.]

[56] RHWJ Ditchfield, W J_ Hehre, and John A Pople. Self-consistent molecular-orbital methods. ix. an extended gaussian-type basis for molecular-orbital studies of organic molecules. *The Journal of Chemical Physics*, 54(2):724–728, 1971. [Cited on page 51.]

[57] Alberto Modelli and Paul D Burrow. Electron attachment to the aza-derivatives of furan, pyrrole, and thiophene. *The Journal of Physical Chemistry A*, 108(26):5721–5726, 2004. [Cited on page 51.]

[58] Adam M Scheer and Paul D Burrow. π^* orbital system of alternating phenyl and ethynyl groups: Measurements and calculations. *The Journal of Physical Chemistry B*, 110(36):17751–17756, 2006. [Cited on pages 51, 59, and 70.]

[59] Kristine Pierloot, Birgit Dumez, Per-Olof Widmark, and Björn O Roos. Density matrix averaged atomic natural orbital (ano) basis sets for correlated molecular wave functions. *Theoretica chimica acta*, 90(2-3):87–114, 1995. [Cited on page 51.]

[60] Rosendo Pou-Amérigo, Manuela Merchán, Ignacio Nebot-Gil, Per-Olof Widmark, and Björn O Roos. Density matrix averaged atomic natural orbital (ano) basis sets for correlated molecular wave functions. *Theoretica chimica acta*, 92(3):149–181, 1995. [Cited on page 51.]

[61] M Gerhards, W Perl, and K Kleinermanns. Rotamers and vibrations of resorcinol obtained by spectral hole burning. *Chemical physics letters*, 240(5-6):506–512, 1995. [Cited on page 52.]

[62] MJEA Frisch, GW Trucks, H Bernhard Schlegel, Gustavo E Scuseria, Michael A Robb, James R Cheeseman, Giovanni Scalmani, Vincenzo Barone, Benedetta Mennucci, GAea Petersson, et al. Gaussian 09, revision d. 01, 2009. [Cited on pages 52 and 55.]

[63] Piotr Skurski, Maciej Gutowski, and Jack Simons. How to choose a one-electron basis set to reliably describe a dipole-bound anion. *International Journal of Quantum Chemistry*, 80(4-5):1024–1038, 2000. [Cited on page 53.]

[64] Ignacio Fdez. Galvan, Morgane Vacher, Ali Alavi, Celestino Angeli, Francesco Aquilante, Jochen Autschbach, Jie J Bao, Sergey I Bokarev, Nikolay A Bogdanov, Rebecca K Carlson, et al. Openmolcas: From source code to insight. *Journal of chemical theory and computation*, 15(11):5925–5964, 2019. [Cited on page 53.]

[65] Rosendo Pou-Amérigo, Luis Serrano-Andrés, Manuela Merchán, Enrique Ortí, and Niclas Forsberg. A theoretical determination of the low-lying electronic states of the p-benzosemiquinone radical anion. *Journal of the American Chemical Society*, 122(25):6067–6077, 2000. [Cited on page 53.]

[66] Seiji Tsuzuki, Kazumasa Honda, Tadafumi Uchimaru, Masuhiro Mikami, and Kazutoshi Tanabe. Origin of attraction and directionality of the π/π interaction: model chemistry calculations of benzene dimer interaction. *Journal of the American Chemical Society*, 124(1):104–112, 2002. [Cited on page 56.]

[67] Jungwun Hwang, Brent E Dial, Ping Li, Michael E Kozik, Mark D Smith, and Ken D Shimizu. How important are dispersion interactions to the strength of aromatic stacking interactions in solution? *Chemical Science*, 6(7):4358–4364, 2015. [Cited on page 56.]

[68] Josué S dos Santos, Romarly F da Costa, and Márcio T do N Varella. Low-energy electron collisions with glycine. *The Journal of chemical physics*, 136(8):02B616, 2012. [Cited on page 65.]

[69] Larry A Curtiss, Paul C Redfern, and Krishnan Raghavachari. Gaussian-4 theory using reduced order perturbation theory. *The Journal of chemical physics*, 127(12):124105, 2007. [Cited on page 66.]

[70] Alessandra S Barbosa, Diego F Pastega, and Márcio HF Bettega. Shape resonances in the elastic scattering of slow electrons by pyridine. *Physical Review A*, 88(2):022705, 2013. [Cited on page 67.]

[71] Prasanga Palihawadana, James Sullivan, Michael Brunger, Carl Winstead, Vincent McKoy, Gustavo Garcia, Francisco Blanco, and Stephen Buckman. Low-energy elastic electron interactions with pyrimidine. *Physical Review A*, 84(6):062702, 2011. [Cited on page 67.]

[72] Eliane M de Oliveira, Sergio d'A Sanchez, Márcio HF Bettega, Alexandra PP Natalense, Marco AP Lima, and Márcio T do N Varella. Shape resonance spectra of lignin subunits. *Physical Review A*, 86(2):020701, 2012. [Cited on pages xviii, 72, and 76.]

[73] KD Jordan, JA Michejda, and PD Burrow. Electron transmission studies of the negative ion states of substituted benzenes in the gas phase. *Journal of the American Chemical Society*, 98(23):7189–7191, 1976. [Cited on pages xviii and 72.]

[74] Roustem V Khatymov, Mars V Muftakhov, and Victor A Mazunov. Phenol, chlorobenzene and chlorophenol isomers: resonant states and dissociative electron attachment. *Rapid communications in mass spectrometry*, 17(20):2327–2336, 2003. [Cited on pages 72 and 76.]

[75] Fabris Kossoski, MHF Bettega, and MT do N Varella. Shape resonance spectra of uracil, 5-fluorouracil, and 5-chlorouracil. *The Journal of chemical physics*, 140(2):024317, 2014. [Cited on page 74.]